Continuous dynamics of cooperation and competition in social foraging

Darius Lewen[1,3†], Vladyslav Ivanov[2†], Jonas Dehning[1,3†], Johannes Ruß[3], Anna Fischer[3], Lars Penke[3], Anne Schacht[3], Alexander Gail[2,3], Viola Priesemann[1,3‡*], Igor Kagan[2‡*]

[1] Max Planck Institute for Dynamics and Self-Organization, Am Faßberg 17, Göttingen, Germany.
[2] German Primate Center – Leibniz Institute for Primate Research, Kellnerweg 4, Göttingen, Germany.
[3] University of Göttingen, Wilhelmsplatz 1, Göttingen, Germany.

† These authors contributed equally to this work.
‡ These senior authors also contributed equally to this work.
* Corresponding authors: viola.priesemann@ds.mpg.de, ikagan@dpz.eu

Abstract

Real-life social interactions often unfold continuously and involve dynamic cooperation and competition, yet most studies rely on discrete games that do not capture the adaptive and graded nature of continuous sensorimotor decisions. To address this gap, we developed the Cooperation–Competition Foraging game — a novel, ecologically grounded paradigm in which pairs of participants (dyads) navigate a continuous shared space under face-to-face visibility, deciding in real-time to collect rewarded targets either individually or jointly. Dyads spontaneously converged on distinct stable strategies along the cooperation-competition spectrum, forming three similarly sized groups: cooperative, intermediate, and competitive. Despite the behavioral complexity, our computational model, which incorporated travel path minimization, sensorimotor communication, and recent choice history, predicted dyadic decisions with 87% accuracy, and linked prediction certainty with ensuing dynamics of spatiotemporal coordination. Further modeling revealed how sensorimotor factors, such as movement speed and skill, shape distinct strategies and payoffs. Crucially, we quantify the cost of cooperation, demonstrating that in many dyads prosocial tendencies outweigh the individual benefits of exploiting skill advantages. Our versatile framework provides a predictive, mechanistic account of how social and embodied drivers promote the emergence of dynamic cooperation and competition, and offers rigorous metrics for investigating the neural basis of naturalistic social interactions, and for linking personality traits to distinct strategies.

Keywords: cooperation, competition, sensorimotor communication, continuous interaction, foraging, value-based decision-making, transparent games

Introduction

In social situations, people and animals often face choices that require balancing or alternating between cooperative and competitive strategies. Whether foraging for resources, hunting, or engaging in economic exchanges, the dynamics of cooperation and competition play a crucial role in determining outcomes such as efficiency, fairness, and overall success. In *dyadic* interactions — involving two individuals — each must evaluate not only their own goals and actions but also the intentions and actions of their partner. These interactions often unfold continuously in time and space, grounded in real-time, embodied decision-making. Understanding how such decisions are made, and what factors drive cooperation or competition, is essential for unraveling the fundamentals of social behavior [1–4]. Here, we elucidate the behavioral and computational mechanisms of continuous, embodied dyadic foraging, using a novel paradigm where human participants can freely choose cooperative, competitive, and intermediate strategies.

Studies relying on classical game-theoretical approaches have elucidated behavioral, computational and neural mechanisms of discrete strategic interactions [5–10]. Yet, even in such repeated ("iterated") interactions, we are often uncertain about whether others intend to compete or cooperate, and how to flexibly adjust strategies in such volatile situations [11]. Due to discrete game formulations inherent to most games, prior research mainly focused on a binary dichotomy between competition and cooperation [12]. While some resource allocation paradigms, such as the Ultimatum, Dictator, Trust and Public Goods games, might involve gradual options (e.g., how much to share) [13, 14], typical 2×2 matrix games involve binary choices. Competitive zero-sum games and pure coordination games allow for only one meaningful strategy, and even in mixed-motive dilemmas such as Prisoner's Dilemma, Stag Hunt, and Chicken / Hawk-Dove, on every trial, or game round, decisions are reduced to a stereotyped binary choice between cooperation and selfish defection. Yet, real-world decisions often transcend such dichotomies [15]. To enable a continuous spectrum of strategies that more accurately reflect the non-dichotomous nature of social decisions, a recent study developed a novel social game called the Space Dilemma, where pairs of participants are presented with a spatial choice on a continuous one-dimensional scale between cooperation and competition [16]. The continuous nature of this game is however limited to a single choice in each discrete trial, where each participant makes an isolated decision informed by the history of previous outcomes and predictions about their partner's upcoming decisions.

To capture the continuous complexity of realistic interactions — in both time and space — less structured and more dynamic pacing and flow are needed. Unlike discrete "simultaneous" and sequential turn-based games, natural social exchanges typically rely not only on predictions from past experience, but also on real-time, moment-to-moment information [17–19]. In animals, simple forms of associative learning are compromised when decisions are temporally separated from their consequences [20], and even in cognitively advanced nonhuman primates, coordination based on mutual choice history is more demanding than relying on the immediately observable actions of others [21–25]. Supporting these findings, theoretical simulations indicate that cooperative populations evolve more easily when there is a continuous flow of information between agents [19], and that action visibility enhances cooperation in coordination games [26]. Likewise, transitioning from discrete to continuous repeated interactions promotes greater cooperation in humans [27, 28], and synchronous action fosters cooperative economic exchanges by strengthening social bonds [29]. At the same time, factors such as action visibility and movement timing may play an equally significant role in shaping competitive strategies [24, 30–32]. More generally, individual dispositions and psychological traits can lead to biases towards being more cooperative or more competitive, independent of the payoff formulation [33]. These biases might be especially prominent in continuous spatiotemporal environments, where immediate face-to-face and action visibility can strongly influence strategic considerations [24, 34–38]. Together, these findings highlight the new insights and possibilities gained by shifting from discrete to continuous decision-making paradigms [39].

Importantly, the transition to continuous interactions does not merely influence strategies; it also enables ethologically grounded, fundamental link between decision-making and sensorimotor control [40]. In *continuous action spaces*, choices are not solely driven by abstract

computations of expected payoffs, but are interwoven with ongoing perceptual and motor processes [41–44]. Unlike the classical serial models in which decisions precede actions, continuous interactions reflect naturalistic "decide-while-acting" scenarios, where concurrent perception, action selection and execution are integrated [45–48]. The dynamic feedback loops between observation and response allow individuals to flexibly adjust their decisions based on environmental cues and the actions of others, facilitating coordination and amplifying or mitigating cooperative or competitive inclinations depending on moment-to-moment evidence.

Real-world constraints, such as effort expenditure and biomechanical limitations, further shape sensorimotor decisions and actions [49–51]. These embodied factors are particularly deeply rooted in foraging behaviors, where the trade-off between effort and reward is a key principle [52, 53]. Foraging demands continuous adjustments to environmental feedback, with physical capabilities and perception-action coupling influencing decisions alongside more abstract cognitive computations [54–57]. The dynamic balance between cognitive effort, physical effort, and expected reward underscores embodied constraints determining foraging efficiency. As a result, decisions in spatially and temporally rich environments emerge from a combination of deliberate strategies and sensorimotor-driven adjustments [58, 59].

Here, we explore the intricate interplay between reward, effort, cooperation and competition, focusing on how strategies emerge and are maintained during economic decision-making in a continuous dyadic foraging context. To this end, we developed a new paradigm called "Cooperation–Competition Foraging" game that affords both classes of interactions between two participants who can collect rewards together or independently. This game capitalizes on the "transparent games" framework that incorporates mutual visibility of partner's ongoing actions [24, 26]. By examining the spatiotemporal movement trajectories and strategic choices made by participants, we seek to capture basic cognitive processes that underpin these dynamic decisions.

Engaging game-like paradigms are increasingly used to study cognition [60, 61]. In line with this approach, we designed our task as a free-flowing social game, in which two participants use continuous arm movements to collect targets in a real-time face-to-face setting enhanced by compelling, dynamic audiovisual feedback. We hypothesized that this game would engender a broad range of strategic interactions. On the one hand, the "gamified" environment combined with real monetary incentives could stimulate competitive tendencies. Conversely, the immediacy of face-to-face engagement and continuous game flow could promote the inherent prosocial cooperativeness and propensity for fairness that characterizes many human interactions [62]. We anticipated that past dependency and information flow would be higher during cooperative behaviors to facilitate coordination, compared to competitive interactions. In particular, we predicted that cooperative behaviors would involve more leader-follower dynamics and reciprocal turn-taking [24], compared to competitive behaviors. More generally, we expected behavior to reflect short timescales of information integration [63], as the real-time action visibility enables participants to adapt dynamically in direct response to their counterparts.

Results

A novel, transparent dyadic foraging game

To study interactions in a controlled setting, we recruited 62 pairs of human participants (dyads) who sat face-to-face across a large transparent bidirectional visual display and played the foraging game together on a two-dimensional (2D) field (Fig. 1a; we recommend viewing the setup and gameplay demo videos for a clearer understanding of the experimental procedures and interaction dynamics: Supplementary Movies). The game reflects the real-world nature in being continuous — both in time and in 2D space — and in enabling the dyads to choose between various levels of cooperation or competition when foraging. Hence, we name it a *Cooperation–Competition Foraging* (CCF) game. Each participant used a mouse-controlled cursor as a virtual agent visible to both participants. At any moment, there were three randomly positioned targets on the screen (Fig. 1b, left) visible to both participants: one "single target" that could be collected by a single agent (worth 0.07€), and two "joint targets" that could only be collected together, but have asymmetric payoffs (providing 0.05€ to one, and 0.02€

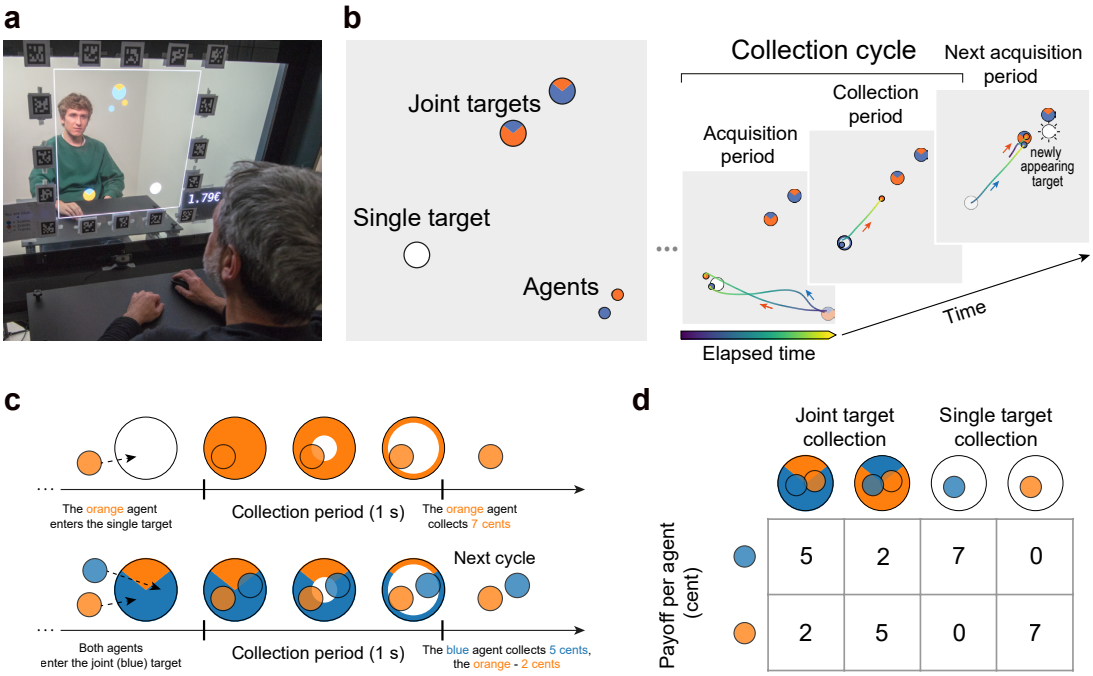

Fig. 1 | Experimental setup and the game. See Movie S1, YouTube, OSF. (**a**) Two participants playing the Cooperation–Competition Foraging (CCF) game on a transparent OLED screen, in front of each other. **Note:** the people depicted here are authors, the people shown in the Movie S1 are lab members, and all have provided explicit consent and are only shown for illustrative purposes. (**b**) Left: Game depiction. Small blue and orange circles are the two cursors ("virtual agents") controlled by the participants with a computer mouse. Agents collect targets (larger circles) by hovering over them. Each agent can collect the white target ("single target") on their own, while the colored targets ("joint targets") can only be collected cooperatively — when both agents hover over it simultaneously. If both agents arrive at a single target, the agent who first reaches the target wins. Right: Game progression. Each collection cycle begins with an acquisition period that lasts until one or both agents select a target. During the subsequent collection period, if a single target is collected as in this example, the free agent can move around. Immediately after the target's disappearance at the end of the collection, the target reappears at a random position, and the next cycle begins. The color of trajectories represents elapsed time from the start of the period (visualizing the relative timing of the two agents: e.g., in the third frame the blue agent begins moving after the orange agent). (**c**) An agent (or both agents) enters the target and hovers over it for 1 s to collect it. Once the collection of the white single target starts, it changes to the color of the collecting agent. The expanding transparent circle from the target's center indicates the collection progress. At the end of each collection cycle, the sound is played and the display of total earnings in € is incremented. (**d**) Payoff matrix. The payoffs of the two participants in each cycle depend on the type of target collection.

to the other agent, or vice versa) (Fig. 1c, d). By design, only one target can be collected at any time. Once a target is collected — requiring one agent for single targets or both agents for joint targets to remain on it for one second — it reappears at a random location on the playing field, initiating the next collection cycle (Fig. 1b, right). Crucially, the locations of the agents and the remaining two targets are not reset, preserving spatial continuity and allowing interactions to unfold naturally across successive cycles.

Although the single targets are designed to elicit a competitive element, we do not call them "competitive" because they can also be used cooperatively (see later). Nonetheless, since such cooperative strategy appeared only in one dyad, we refer to the dyads that mainly collected single targets as competitive, and to those that mainly collected joint targets as cooperative if not stated otherwise.

To avoid introducing an *a priori* bias towards the single or joint targets, we assigned the same *joint payoff* (i.e. the sum of payoffs for both participants) for both target types. Participants were informed about the corresponding payoffs (Fig. 1d) and were instructed to

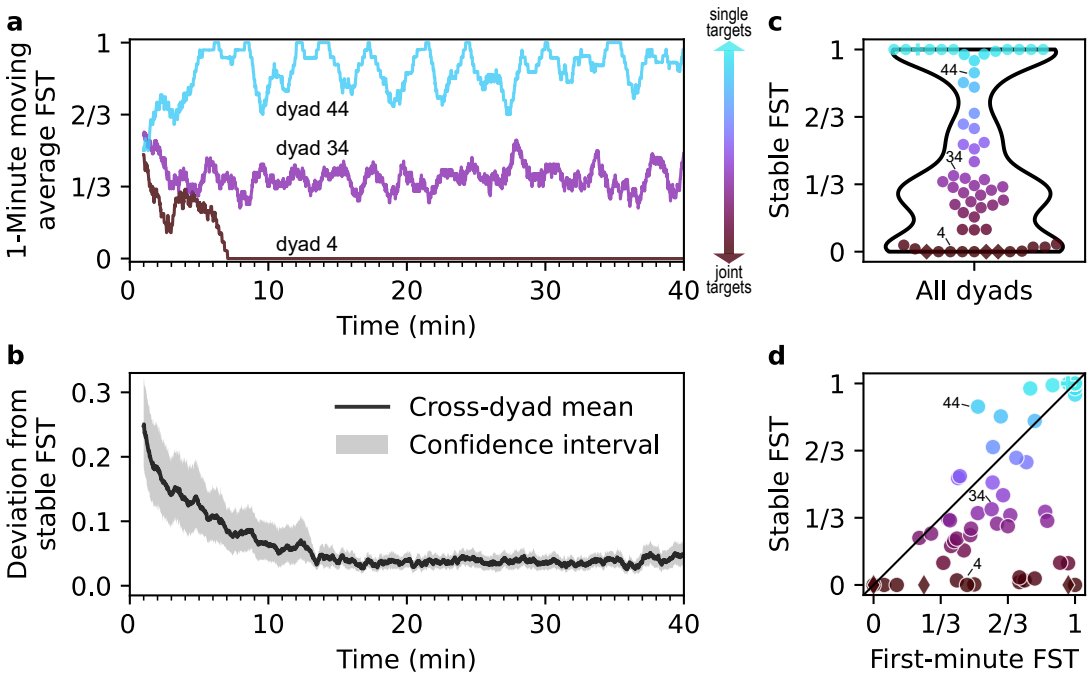

Fig. 2 | Each dyad converges to a specific stable strategy on the cooperation–competition spectrum. (**a**) Moving average (1 min window) of the *fraction of single targets* (FST) for three representative dyads. (**b**) Mean absolute deviation from a dyad's eventual stable strategy as a function of time. After 14 minutes, all 58 included dyads have converged to a stable FST. (**c**) Distribution of the stable FST across dyads, which we categorize into three groups: largely cooperative, preferentially collecting joint targets (FST ≤ 0.1, n=14, Movie S2, YouTube, OSF), largely competitive, preferentially collecting single targets (FST ≥ 0.9, n=14, Movie S4, YouTube, OSF), and an intermediate, performing mixed collections ($0.1 <$ FST < 0.9, peaking around $\simeq 1/3$, n=30, Movie S3, YouTube, OSF). Colors along the vertical axis represent the stable FST of each dyad, from brown to cyan. Here and in (D), the non-dot markers (plus, diamonds) indicate special strategies described later. (**d**) First-minute FST vs stable FST (from 10 to 40 min). Most dyads decrease their FST (i.e. become more cooperative) over time.

collect as many targets as possible, to earn their payment. To make the game more realistic by introducing a "travel cost", and avoid a total payoff being uniquely dependent on skill, the maximal movement speed was limited. If the limit was exceeded, the agent's position (cursor) lagged relative to the mouse until they slowed down.

After a short initial practice to familiarize themselves with the game mechanics, participants played two 20-minute blocks and were rewarded by the cumulative payoffs collected in one randomly chosen block. By situating foraging within a salient social context and transporting it to a shared virtual field, this setup provided a controlled yet rich dynamic environment, well suited to investigate how dyads develop cooperation or competition when collecting single and joint targets.

Dyads converge to stable strategies on the cooperation–competition spectrum

Due to the continuous and open nature of the game, we expected a variety of strategies to emerge. Indeed, most dyads, after an initial transient, converged to a specific set-point on the cooperation–competition spectrum, as represented by a relatively stable *fraction of single targets* (FST; defined as the number of single targets collected over a certain period divided by the number of all targets collected over the same period; Fig. 2a). We found that all but 4 (58/62) dyads exhibited a stable FST after the 14 min period (Fig. 2b), and most dyads converged within 10 minutes. Therefore, we excluded the first 10 minutes and used the remaining

relatively stable 30 minutes of interaction (1.5 blocks) for our analysis, to focus on stable strategies. The 4 dyads that abruptly changed their FST after the initial convergence period were excluded from further analysis. Interestingly, most dyads that changed their FST during the initial period became more cooperative during this time (Fig. 2d). After convergence, dyads were distributed along the entire FST axis (Fig. 2c). But the FST distribution is not uniform — dyads can be categorized into three "groups" along the continuum of FST: (1) cooperative dyads that mainly coordinate to collect joint targets (FST ≤ 0.1), (2) dyads that mostly compete for single targets (FST ≥ 0.9), and (3) dyads with intermediate, yet stable, strategies ($0.1 <$ FST < 0.9, with a peak around FST $\simeq 1/3$). The spontaneous emergence of the three apparent groups raises the question about the strategies underlying the choices along the cooperation–competition spectrum.

Path minimization and cooperation–competition ratio shape dyadic strategies

To build a theoretical foundation for describing the observed strategies, we derive the optimal dyad strategy (in terms of joint payoffs) under different assumptions. According to the optimal foraging theory [52, 56], and more generally economic decision theories [50, 64–68], foraging agents need to maximize reward and minimize effort. We expand on these principles for the case of dyadic decisions.

For idealized agents that move in a straight line at the maximal possible speed (which is limited by game design), the distance to the collected target determines the payoffs that can be obtained within a fixed time. If one assumes that both agents always share the same position at the start of each collection cycle, then selecting the closest among three potential targets implements path minimization (Fig. 3a). Minimizing the path leads, due to the random target placement, to an optimal FST of exactly $1/3$ (Fig. 3b, gray curve, middle purple square).

However, an identical positioning of both agents at the start of every collection cycle is not the best strategy for optimizing the joint payoff. Instead, during the collection of a single target, the non-collecting (free) agent can place itself to minimize the expected distance to the next target — thereby contributing cooperatively to joint efficiency, *across* collection cycles. Such "advantageous" placement must satisfy two conditions. First, it should minimize the expected distance from *either* agent to the next randomly appearing single target (Fig. 3c and Fig. S1a). Second, the free agent should not place itself further from the nearest joint target than the currently collecting agent (e.g., stay within the circle around the "blue" joint target in the example in Fig. 3c). Thereby, the free agent does not delay a potential subsequent collection of the joint target (Fig. 3c; Supplementary Methods 1.1). As a consequence of such advantageous placement, the two agents together cover a larger area any agent can reach within a limited time, increasing the probability that collecting the newly-appearing single target will be a better choice than collecting a joint target. Therefore, higher FST values are now yielding better results, with an optimum at FST ≈ 0.55 instead of $1/3$ (simulation results in Fig. 3b, black curve, see also Fig. S1 for details).

It is important to emphasize that this advantageous placement strategy is *not* competitive. It maximizes the joint payoff of a dyad. It is thus a cooperative placement to minimize the expected distance to the next target; but during the acquisition period, both agents might compete again. In a completely competitive strategy, the free agent would not aim at minimizing the expected distance from *either* agent to the single target. Instead, the free agent would aim at optimizing the probability to be nearer to the newly appearing single target than the collecting agent. In practice, this leads to a placement close to the competing agent, but a bit closer to the center of the game field (Fig. S1f).

Despite these clear theoretical optimality results, actual dyads spanned the entire range of FSTs (Fig. 3d), thereby deviating from a simple path-minimizing strategy. Therefore, we explore optimality under the constraint of a specific FST. For each dyad, we introduced a specific weighting factor, representing their manifested preference to choose single versus joint targets (Fig. S2a, "target type weighting"). This weighting factor reflects the overall preference of a dyad for joint or single targets, typically approximating their preference for cooperation or competition. For example, if a dyad prefers joint targets over single targets, they might choose

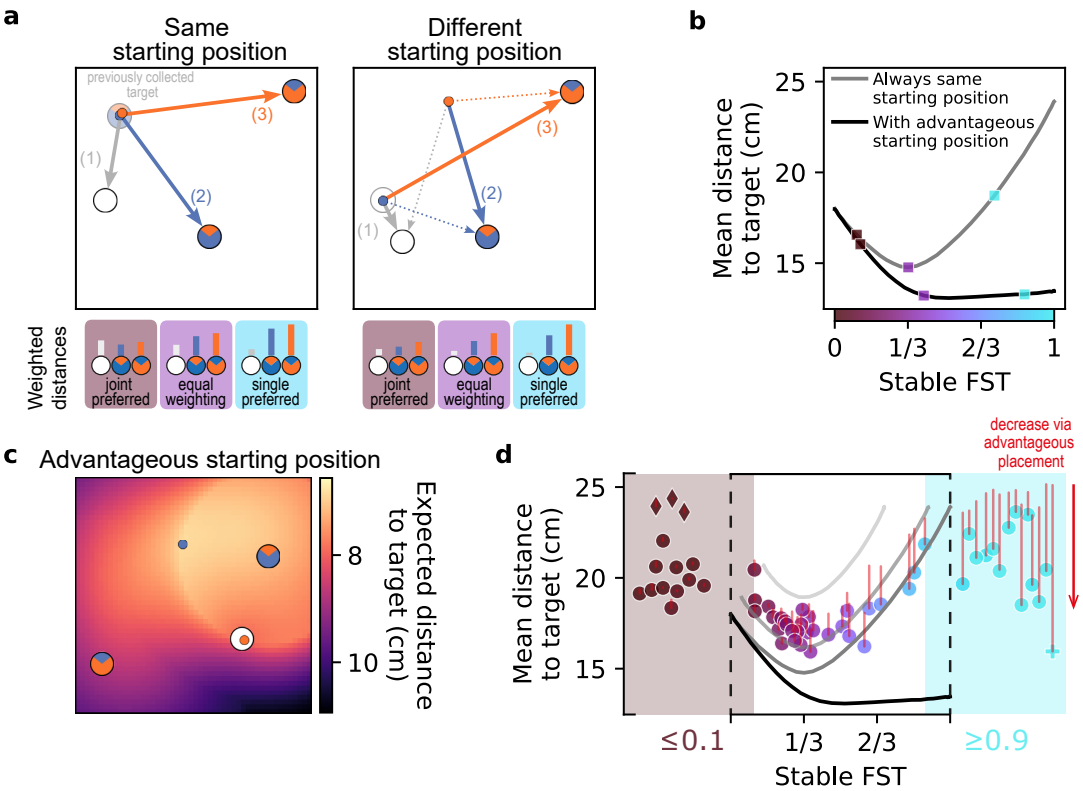

Fig. 3 | Weighted path minimization and advantageous placement. (**a**) Two exemplary initial conditions of weighted path minimization. Three distances are relevant for target selection: for the single target, the shortest distance (1) from either agent; for each joint target, the longest distance (2, 3) from either agent. Irrelevant distances are shown as dotted arrows. Examples of "weighting" these distances by different FST preferences are shown below, where the target with the shortest weighted distance is selected. (**b**) Theoretical optima. Simulating target selection based on differently weighted distances results in differing FST and mean distance to target. The markers correspond to the weightings visualized in colored panels in (a). Simulations are done either with the same starting position as in the left panel in (a) (gray curve) or with advantageous placement (black curve). (**c**) Example of an advantageous placement for one spatial configuration. An advantageous placement is only possible during a single target collection. The free, non-collecting agent (blue in this example) moves into a different starting position that minimizes the expected distance to the next target, indicated by the colormap (see Supplementary Methods 1.1 for details). (**d**) Mean distance to selected target as function of FST. The actual dyads lie between simulated strategies. Two additional lighter gray curves correspond to simulations with the same starting position but when the weighted closest target is chosen in only 70% (upper gray curve) or 90% (middle gray curve) of collection cycles, and a random selection otherwise. The red vertical lines indicate the mean distance reduction due to some degree of advantageous placement, for each dyad. Mostly cooperative dyads (FST ≤ 0.1, brown) and mostly competitive dyads (FST ≥ 0.9, cyan) are plotted separately to illustrate a large vertical spread due to strategies deviating from weighted path minimization, such as turn-taking (diamond markers) and advantageous placement.

a joint target even when the single target was physically the closest (Fig. 3a, brown square). If however the single target is very close, then even a dyad that strongly prefers joint targets might occasionally select the single target (Fig. 3b, brown square).

For each FST, we calculated the optimal strategy — the minimal distance attainable (Fig. 3b), either by assuming simple path minimization (gray curve) or additionally taking into account advantageous placement of the free agent (black curve). While for simple path minimization there is a clear optimum at FST 1/3, there exists a continuum of similarly good strategies for path minimization with additional advantageous placement ($0.4 \leq$ FST ≤ 1; note the nearly flat black curve starting at 0.4 in Fig. 3b). Most actual dyads, however, performed advantageous placement only to a certain degree (Fig. 3d and Fig. S1g). Therefore,

the equal weighting path minimization without advantageous placement can explain the formation of the intermediate group around FST 1/3. For each dyad, we computed the mean distance to the selected target across trials; statistical comparisons between groups were then performed on the distribution of these per-dyad means using nonparametric tests, which assess differences in group-level medians. Indeed, the distance to target in the intermediate group is reduced compared to the cooperative and the competitive groups (Mann-Whitney U test, intermediate vs cooperative: $U = 388, p < 10^{-5}, n_1 = 30, n_2 = 14, \mathrm{Mdn}_1 = 17.52, \mathrm{IQR}_1 = [17.00, 18.30], \mathrm{Mdn}_2 = 20.22, \mathrm{IQR}_2 = [19.36, 21.72], r_{rb} = 0.68, CI = [0.51, 0.8]$; intermediate vs competitive: $U = 367, p < 10^{-4}, n_1 = 30, n_2 = 14, \mathrm{Mdn}_1 = 17.52, \mathrm{IQR}_1 = [17.00, 18.30], \mathrm{Mdn}_2 = 20.78, \mathrm{IQR}_2 = [19.63, 22.21], r_{rb} = 0.60, CI = [0.31, 0.79]$; all tests in this paper are two-sided).

To estimate how well the dyads follow a (weighted) path minimization strategy, for each collection cycle we predicted the subsequent choice of the target (Supplementary Methods 1.1). For non-weighted path minimization, the average choice prediction accuracy across dyads was 59%, and the median 61%, significantly higher than the 33% chance (Fig. 4a, Wilcoxon signed-rank test, $W = 3, p < 10^{-6}, n = 58, \mathrm{Mdn}_1 = 0.61, \mathrm{IQR}_1 = [0.53, 0.68], \mathrm{Mdn}_2 = 0.33, \mathrm{IQR}_2 = [0.33, 0.33], r_{rb} = 0.87, CI = [0.85, 0.87]$). The dyads with intermediate strategies were particularly well predicted (average accuracy 65%; Mann-Whitney U test comparing accuracies of intermediate and non-intermediate dyads, $U = 740, p < 10^{6}, n_1 = 30, n_2 = 28, \mathrm{Mdn}_1 = 0.68, \mathrm{IQR}_1 = [0.62, 0.69], \mathrm{Mdn}_2 = 0.53, \mathrm{IQR}_2 = [0.45, 0.58], r_{rb} = 0.65, CI = [0.49, 0.79]$), suggesting that the intermediate dyads often perform true (non-weighted) path minimization. For the weighted path minimization, the average choice accuracy increased to 78% across all dyads (Fig. 4a, Wilcoxon signed-rank test comparing non-weighted vs weighted minimization, $W = 21, p < 10^{-6}, n = 58, \mathrm{Mdn}_1 = 0.61, \mathrm{IQR}_1 = [0.53, 0.68], \mathrm{Mdn}_2 = 0.75, \mathrm{IQR}_2 = [0.69, 0.88], r_{rb} = 0.85, CI = [0.79, 0.87]$). Thus, a substantial portion of the observed dyadic strategies can be accounted for by combining simple path minimization with differential weighting of joint versus single targets.

Beyond weighted path minimization: social and sensorimotor planning factors

Although weighted path minimization — both within and across collection cycles — already accounts for 78% of choices, we identified additional factors that further enhance predictive accuracy. Analyses revealed that actual moving average FST fluctuations are typically smaller than expected from the weighted path minimization (Fig. 4c, Fig. S3a), suggesting that dyads use more sophisticated strategies. Specifically, during single target collections, the free agent that is currently not collecting the single target often positioned itself onto one of the joint targets, effectively *inviting* the subsequent, cooperative joint target collection in the next cycle (Movie S5, YouTube, OSF). Another prevalent pattern exhibited by many dyads in the cooperative and intermediate groups was a tendency to avoid the newly appearing target.

To account for these patterns, we incorporated invitations and the identity of the two previously collected targets as across-cycle predictors in a generalized linear model (GLM), in addition to the weighted path minimization. This model, calculated separately for each dyad, predicts the next collected target at the start of each acquisition period. The mean prediction accuracy improved compared to the weighted path minimization from 78% to 87% (Fig. 4a, Wilcoxon signed-rank test, $W = 14, p < 10^{-6}, n = 58, \mathrm{Mdn}_1 = 0.75, \mathrm{IQR}_1 = [0.69, 0.88], \mathrm{Mdn}_2 = 0.84, \mathrm{IQR}_2 = [0.81, 0.98], r_{rb} = 0.79, CI = [0.70, 0.84]$). The model improvement (AIC) due to inclusion of across-cycle predictors was apparent in the cooperative group in contrast to the competitive group (Fig. 4b, Mann-Whitney U test, $U = 15, p < 10^{-4}, n_1 = 14, n_2 = 14, \mathrm{Mdn}_1 = 126.92, \mathrm{IQR}_1 = [75.49, 338.49], \mathrm{Mdn}_2 = -8, \mathrm{IQR}_2 = [-8, 6.54], r_{rb} = 0.72, CI = [0.49, 0.84]$), and it was even more pronounced in the intermediate group ($U = 128, p < 0.05, n_1 = 14, n_2 = 30, \mathrm{Mdn}_1 = 126.92, \mathrm{IQR}_1 = [75.49, 338.49], \mathrm{Mdn}_2 = 317.03, \mathrm{IQR}_2 = [270.85, 395.15], r_{rb} = 0.31, CI = [0.03, 0.64]$).

The GLM coefficients quantifying the effect of invitations are statistically significant in 30 dyads, with 29 showing a positive effect (Wald tests, here and further: $p < 0.05$, Benjamini-Hochberg-adjusted across 58 dyads). Thus, there is a significant increase in the

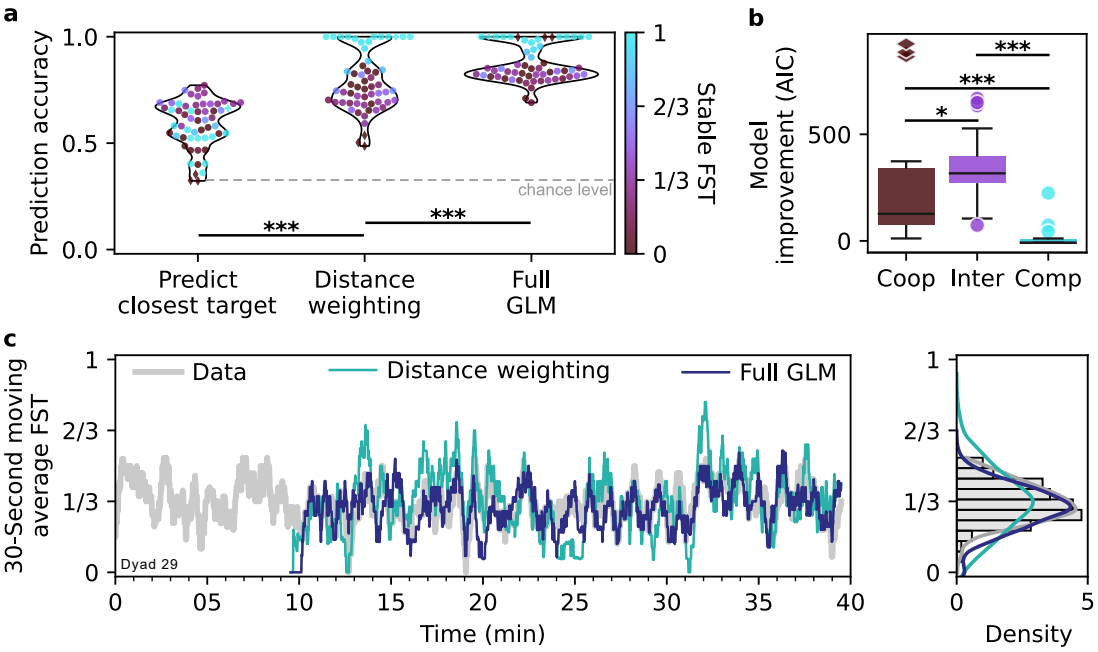

Fig. 4 | Cooperation/competition-weighted path minimization and across-cycles predictors explain dyadic target choice. (**a**) Predicting the choice of the next target, using (i) the closest distance, (ii) the weighted closest distance or (iii) the "full" generalized linear model (GLM). The full GLM, which includes across-cycles predictors such as target choice history and *invite placements*, explains the dyads' choices in 87% of collection cycles. (**b**) Model improvement (Akaike information criterion, AIC) when including across-cycles predictors, shown as box-and-whisker plots (median, interquartile range, min/max, and outliers). Integrating recent choice and social information, represented by across-cycle predictors, improves the prediction in the cooperative group (Coop) and is even more pronounced in the intermediate group (Inter), compared to the competitive group (Comp). (**c**) Timecourse of actual and predicted FST (moving average over target choice prediction in one exemplary dyad). While the random target placement drives the fluctuations around the mean FST (left panel), incorporating the full GLM better matches the observed variance (right panel, see Fig. S3 for population data).

collection probability of the invited joint target across dyads (binomial test, $proportion = 0.97, 95\%\ CI\ [0.82, 0.99], Z = 4.9, p < 10^{-6}$). Note that in the case of an invite, the previously collected target is a single target that is subsequently avoided. The effect of avoiding the previous target is also clear if the previous target is a joint target (Wald tests, $p < 0.05$ in 37 dyads) but is inconsistent when the previous target is a single target and no invite is present. In the latter case, the GLM coefficients indicate a significant (Wald tests, $p < 0.05$) tendency to avoid the previous single target for 14 dyads but also a significant increase in the single target collection probability for 9 dyads (no consistent effect across dyads, binomial test, $proportion = 0.61, CI\ [0.38, 0.80], Z = 0.83, p = 0.43$). Thus, beyond cooperation/competition-weighted path minimization, additional planning factors across cycles - invitations and previous target identities - shape the dyadic strategies.

The prediction improvement introduced by these additional factors is also apparent in the time course of the actual and predicted FST. In contrast to the weighted distance prediction, the "full" GLM captures the dyads moving average FST fluctuations better (Fig. 4c, Fig. S3, Wilcoxon signed-rank test comparing the differences of standard deviations between 30-second moving average FST of the actual and each of the two model's predictions for the 40/58 dyads that exhibited FST fluctuations, $W = 258, p < 0.05, n = 40, \mathrm{Mdn}_1 = -0.01, \mathrm{IQR}_1 = [-0.03, 0.02], \mathrm{Mdn}_2 = 0.0008, \mathrm{IQR}_2 = [-0.009, 0.02], r_{rb} = 0.32, CI = [0.04, 0.62]$). In other words, with few exceptions dyads primarily follow cooperation–competition weighted path minimization, but if the random target placement sequence happens to dictate a substantial deviation from their established mean FST, the across-cycle predictors come into play. For example, if weighted path minimization prompts several single target collections in a row, real

participants would perform an invite leading to the collection of a joint target, and thus avoid a potential breakdown of established cooperation.

These findings highlight the influence of social and sensorimotor planning factors that extend beyond a cooperation–competition weighted path minimization. We propose that the observed reluctance to repeat the same target type reflects a dual contribution: a sensorimotor bias favoring prospective planning and coordination for already visible targets [47, 69], and a social motivation for fairness. The latter is especially pronounced in the extreme case of three exclusively cooperative dyads (FST = 0), who exhibited strict turn-taking behavior between the two joint targets (Fig. 4a, diamond markers, Movie S6, YouTube, OSF).

Likewise, the invitations represent one of the most basic forms of *sensorimotor communication* [70]. During the collection of a single target — primarily a competitive act — the non-collecting agent conveys a compelling social signal for cooperation by placing itself on a joint target. Indeed, our findings reveal that these invitations are accepted in the majority of cases (88%), even when the new single target is closer (79%). This indicates that beyond path minimization, invitations play an important additional role in shaping intermediate strategies, highlighting the interplay between social signaling and strategic decision-making.

Choice certainty shapes ensuing spatiotemporal interactions

Thus far, our analyzes dealt with the prediction of discrete target choices at the beginning of each collection cycle. However, these choices are the result of sensorimotor interactions in the continuous action space. Here, we link the choice modeling to the classification of spatiotemporal trajectories, to characterize ongoing decision processes and dyadic coordination. Beyond the prediction of the discrete target choices in each cycle, we derive the certainty of this prediction, measurable via its entropy. This choice certainty represents an estimate of how sure the participants are about their next move, given the current spatial contingencies and dynamics across collection cycles as modeled by the GLM. Note that for this analysis, we exclude the dyads that mostly collected single targets (FST ≥ 0.9) since there is always a high certainty in their target choice. To relate target choice certainty to ensuing dynamics that precede and determine the subsequent collection, we analyzed the ongoing decision processes reflected in spatiotemporal trajectories. We classified the collection cycles into several representative classes, associated with different levels of apparent coordination (Fig. 5a; Supplementary Methods 1.3).

One prominent class of high coordination is the already mentioned *invitations*, where one agent places itself on a joint target in advance. This invitation could be reciprocated — the other agent moving towards it — or denied, leading to a "failed invitation". By definition, the invitations can only take place in dyads that collect single targets as well as joint targets from time to time. The next two classes are characterized by a *movement towards the same* (either single or joint) target. Following the collection of the previous target, the agents move simultaneously to the next target ("concurrent to the same target"), or one agent leads and the other follows ("one ahead to the same target"). Third, the trajectories could be "strongly curved", due to starting a preemptive movement before the choice is made [43, 44], initial miscoordination, or multiple changes of mind (Movie S7, YouTube, OSF). Lastly, one of the agents could select a joint target while the other would go to collect a single target (denoted here by "different targets").

The above classification is performed separately for each collection cycle. Given the continuous transition between the cycles, we explored the across-cycles transition probabilities, using Markov chain representation. The most prominent node is the "concurrent to same target": it is the most probable class after any type of interaction except when the invitation is present but not yet reciprocated. These miscoordinations, "different targets" and "failed invitation", elicit a social pressure and are typically corrected by the subsequently accepted "invitation". Such invitations are often *passive* (54% of all invitations) — the inviting agent communicates by remaining on the joint target they entered previously. The other 46% are *active* invitations, taking place after both agents aimed for the single target (concurrent or one ahead). Thus, we can divide the invitations into passive and active sensorimotor communication.

By relating the trial classes to the target choice uncertainty of GLM predictions, we found that higher uncertainty is associated with a higher prevalence of less coordinated interactions

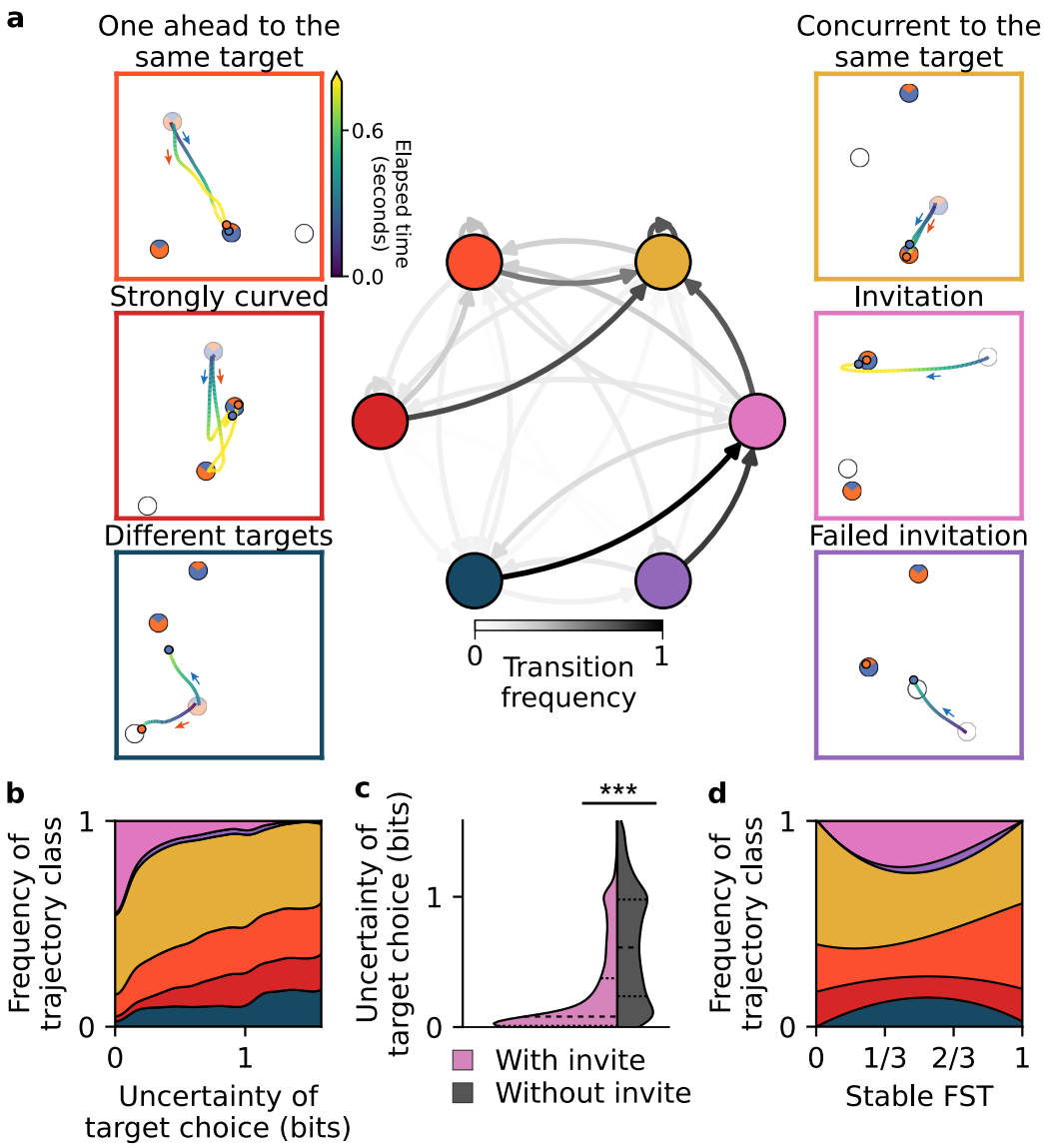

Fig. 5 | High uncertainty of target choice increases the probability of uncoordinated trajectories. (**a**) We classify the trajectories within each collection cycle into different classes (outer panels; the color of the trajectory represents the time from the start of the collection cycle, the faded targets are the targets collected in the preceding cycle). Transition probabilities are shown using a Markov chain (inner panel). (**b**) Distinct fractions of trajectory classes are observed across varying levels of target choice uncertainty, as estimated by the full GLM. Trajectories associated with miscoordination or failed prediction of the partner's choice ("Strongly curved" and "Different targets") are often apparent when the model has a higher uncertainty. In contrast, trajectories with high coordination between agents (accepted "Invitations" and "Concurrent to the same target") are predominant at low model uncertainties. Trajectory classes are denoted by the same color as in (a). (**c**) After an invite by sensorimotor communication the uncertainty about target choice is significantly reduced. (**d**) Average frequency of trajectory classes as a function of stable fraction of single targets (FST). Note that in (a) (inner panel), (b) and (c) only dyads with non-negligible target choice uncertainty are included (FST < 0.9).

(Fig. 5b). In some situations of high uncertainty, dyads manage to maintain coordination, either by one agent moving ahead and signaling the next target ("one ahead to same target"), or by multiple trajectory adjustments leading to "strongly curved" trajectories. In other situations, however, high uncertainty leads to a breakdown of coordination ("different targets"). In contrast to these classes, the mean uncertainty of collection cycles classified as invitation

is significantly reduced (Fig. 5c, Mann-Whitney U test comparing prediction entropy of initial conditions with and without the invite factor, $U = 7608968, p < 10^{-6}, n_1 = 5948, n_2 = 5948, \mathrm{Mdn}_1 = 0.08, \mathrm{IQR}_1 = [0.01, 0.37], \mathrm{Mdn}_2 = 0.61, \mathrm{IQR}_2 = [0.24, 0.98], r_{rb} = 0.49, CI = [0.48, 0.51]$), demonstrating the utility of salient sensorimotor communication for efficient coordination.

The relation between spatiotemporal dynamics and uncertainty is also apparent in the observed distribution of collection classes over stable FST (Fig. 5d). One of the two classes associated with high uncertainty, "different targets", is peaking at intermediate FSTs, in line with high certainty of target type choice for low and high FST dyads. The other class, "strongly curved", is uniformly distributed because it encompasses multiple components: the uncertainty about which of the two joint targets to select (low FST dyads), which of the three targets to select (intermediate FST dyads), and the uncertainty about position of the next single target (high FST dyads; "go-before-you-know" or "decide-while-acting" effect that refers to when the action starts before the goal is determined [44, 47]; Fig. S4).

More generally, Fig. 5d shows that in high FST dyads, both agents nearly always moved toward the same (single) target, indicating that these participants were indeed *competing*, rather than allowing one another to collect the target.

These analyzes show that our generalized linear model captures, to a large extent, the cognitive processing underlying the ensuing dyadic choices. At the same time, it is remarkable that even at a high model uncertainty, the agents still often exhibit straight, coordinated concurrent movements to the same target. This can be explained, at least in part, by co-evolving online coordination, whereby participants closely observe each other's movements and continuously adjust their trajectories.

Spatiotemporal variables shaping joint payoff

As demonstrated in the preceding sections, real dyads do not always choose the (target type-weighted) nearest target, and they might perform advantageous placement only to a certain degree. Furthermore, real dyads do not always move in straight lines at constant speed. Here, we disentangle the contribution of these deviations from idealized patterns to the obtained payoffs.

In a first approximation, the main contributing factors to the joint payoff are the dyads' average trajectory length and their average speed, which explains why the joint payoff increases as a function of FST up to 1/3 and then stabilizes (Fig. 6a). The payoff in this task is proportional to the total amount of targets collected, which is again approximately proportional to the inverse of the mean collection cycle duration (Pearson's correlation coefficient $r(56) = 0.99, p < 10^{-6}, CI = [0.99, 0.99]$). The mean acquisition duration is well approximated by the limiting agent's mean trajectory length and speed ($r(56) = 0.99, p < 10^{-6}, CI = [0.99, 0.99]$). For single targets, the limiting parameters are the trajectory length and the speed of the agent who collects the target. For joint targets, these parameters are determined by the agent that enters the target last. The resulting trajectory length is a U-shaped function of FST (Fig. 6b). The speed increases with FST (Fig. 6c, $r(56) = 0.71, p < 10^{-6}, CI = [0.55, 0.82]$), demonstrating that more competitive dyads move faster (this result also holds for the average speed of the two agents rather than the agent that won the single target $r(56) = 0.59, p < 10^{-5}, CI = [0.39, 0.73]$). Due to the increased speed, the effect of longer trajectories at high FSTs on payoffs is compensated; therefore, this U-shaped function does not translate to the joint dyad payoffs — the payoff of high FST dyads does not drop (Fig. 6a).

To understand the origins of the observed U-shaped pattern in the trajectory length, we decomposed it into three contributing components. The first component is the distance from the previous to the next target (Fig. 6d). This distance is largely determined by the strategy of weighted path minimization. In most dyads, the mean observed distance is between that of the two simulated scenarios where the closest target (cooperation–competition weighted) is selected in 70% and 90% (Fig. 6d). The highest distances are those of the three turn-taking dyads (diamond markers) who alternated between the two joint targets regardless of the distance. The second component is the additional distance due to performing non-optimal, curved trajectories. This inefficiency played a stronger role in dyads that mainly collect joint targets, due

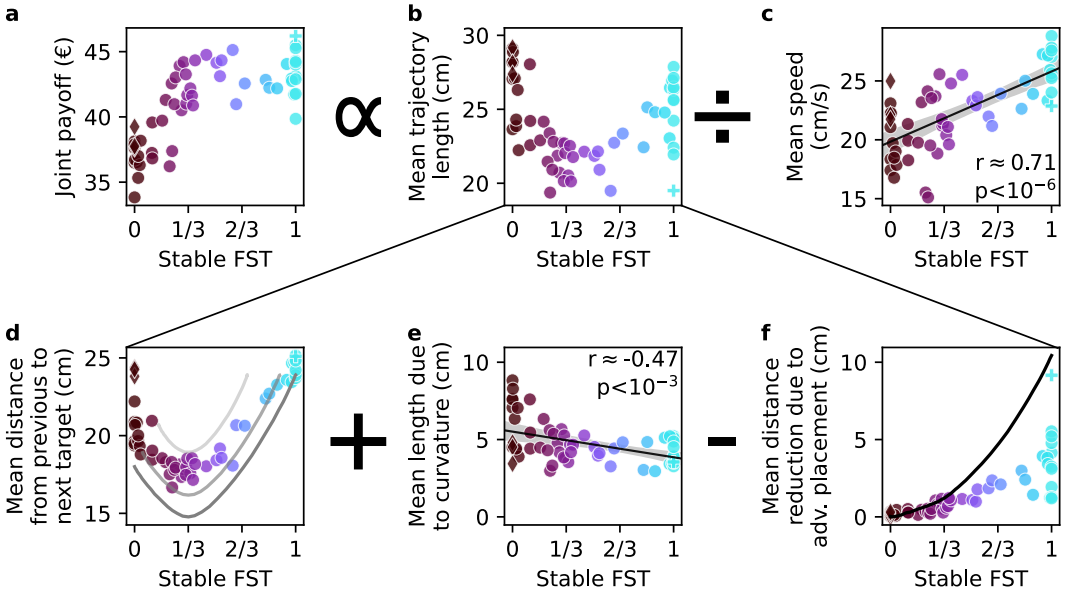

Fig. 6 | Spatiotemporal factors shape the payoff in a continuous action space. (**a**) The joint payoff across both participants in a dyad is proportional to the mean acquisition duration. The mean acquisition duration is well-approximated by dividing the mean trajectory length (**b**) by the mean movement speed (**c**) on these trajectories. Note the increase in speed with higher fractions of single targets (FST). (**d-f**) We subdivide the mean trajectory length in (b) into three components: (**d**) Without advantageous placement, the trajectory length is at least the mean distance from the previous to the next target. The dark gray curve indicates the minimal mean distance attainable for each FST value, the lighter curves indicate the same path-minimizing strategy applied only in 90% and 70% of collection cycles. (**e**) Curved trajectories increase the mean trajectory length, especially at low FST because of potential miscoordination between participants. (**f**) Advantageous placement reduces the trajectory length. To achieve this, the free agent must place itself advantageously during a single target acquisition period. One dyad (plus marker) nearly reaches the maximal attainable distance reduction (black curve, *cf.* Fig. 3d).

to occasional initial miscoordination (Fig. 6e, $r(56) = -0.47, p < 10^{-3}, CI = [-0.65, -0.24]$). The exception to this pattern were the three turn-taking dyads, who eliminated miscoordination through their consistent strategy. The mean curvature is also slightly increased for (some) FST=1 dyads because they start moving even before they perceive where the newly appearing single target is (see Fig. S4 for examples of "go-before-you-know" effect [43]). Last but not least, as described above, while one agent collects a single target, the other, "free" agent can perform advantageous placement, thereby decreasing the mean anticipated trajectory length. As expected, the advantageous placement contribution increased with FST, however most dyads utilized only a fraction of the theoretically possible distance reduction (Fig. 6f). In some dyads the non-collecting agent remains near the other, leading to very little distance reduction (Movie S4, YouTube, OSF). In other dyads, the non-collecting agents place themselves nearer to the center such that they have an advantage in *competing* for the next single target (Fig. S1f, Movie S8, YouTube, OSF), leading to a intermediate distance reduction. Finally, a unique dyad designated by the plus-marker at FST=1 showed a *cooperative*, or at least conflict-avoiding strategy, dividing the game field into a lower and upper half where each agent respectively collected the single targets, resulting in remarkably effective distance reduction (Movie S9, YouTube, OSF).

In conclusion, this decomposition demonstrates how sensorimotor variables shape the payoff distribution, leading to the lower payoff of cooperative dyads (Fig. 6a). The observed cooperative strategies (FST $< 1/3$) come at the cost of (i) longer distances to the next target, (ii) lower speed, (iii) more curved trajectories for some dyads because of initial miscoordination, and (iv) the loss of the optimization opportunity by advantageous placement before the beginning of a collection cycle. More competitive dyads compensate for the longer distances by higher speed and advantageous placement optimizations.

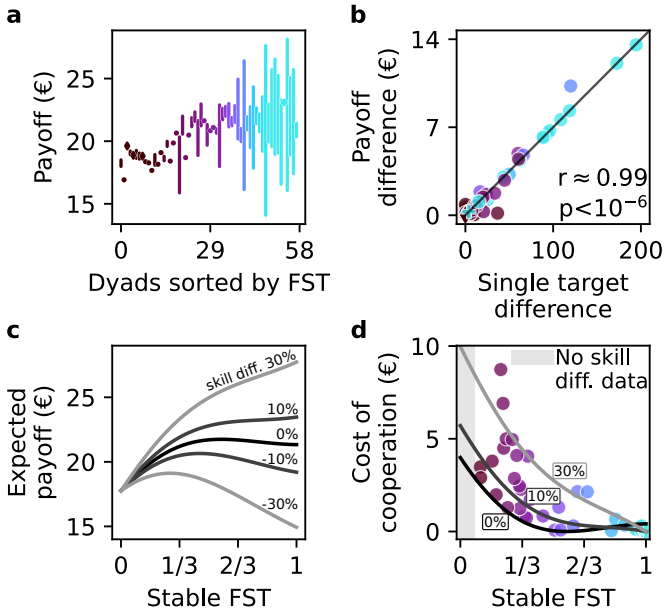

Fig. 7 | Individual payoff, skill difference and cost of cooperation. The optimal individual strategy that maximizes the individual payoff is determined by skill differences, and in general favors collecting single targets. Nevertheless, many participants chose a more cooperative strategy with joint targets and paid a cost of cooperation. (**a**) Individual payoff and difference between participants. Each bar represents the lower and the higher individual payoff in a dyad (bottom and top ends of the bar, respectively); hence, the bar length represents the payoff difference between the participants. If the payoff difference is below 30 cents a marker instead of a bar is used. Dyads are arranged in order of increasing FST. (**b**) The payoff difference within a dyad is mainly determined by the difference in single targets collected by each agent, and only little by a bias towards one or another joint target. (**c**) Estimated payoff depends on FST and skill differences within a dyad. The greater the skill difference (i.e., the difference in single targets collected, normalized by the total number of single targets), the more beneficial competitive strategies become for the higher-skilled participant. Note that the black curve (skill diff. = 0%) corresponds to the half of the average profile for the joint payoff shown in Fig. 6a. (**d**) Estimated loss of payoff, representing the monetary "cost of cooperation" for the higher-skilled participant within a dyad. Despite this cost, many participants still chose to cooperate (lower FST) rather than maximize their economic gain.

Payoff differences between participants, skill and cost of cooperation

Thus far, we considered the joint payoff and the observed strategies at the level of a dyad. However, the two participants in a dyad might differ in several regards, for instance in their ability or willingness to collect single targets, or due to a biased collection of joint targets benefiting one participant. Therefore, here we explore the factors underlying *within-dyad* payoff differences and assess the cost of deviating from individually optimal strategies.

Across dyads, within-dyad payoff difference (ranging from 0 to 14 €; Fig. 7a) correlated with the FST ($r(56) = 0.67, p < 10^{-6}, CI = [0.50, 0.79]$). This correlation was nearly perfectly accounted for by the difference in the number of single target collections between the two agents (Fig. 7b, $r(56) = 0.99, p < 10^{-6}, CI = [0.98, 0.99]$). This difference is largely (82%) due to discrepancies in skill, especially in more competitive dyads (96%) (these numbers are derived from acquisition periods where both agents tried to collect the single target, see classification in Fig. 5). The remaining part of the difference in single targets might reflect varying attitudes toward deviating from cooperation on joint targets in favor of opportunistically pursuing a nearby single target ("different targets" class, see Fig. 5).

We numerically estimated the resulting individual payoff as a function of skill difference and FST (Fig. 7c), assuming the speed and trajectory lengths of the average dyad at the different FSTs. For equal skill, the expected individual payoff corresponds to half of the joint payoff (*cf.* Fig. 6a), showing a flat plateau between FST 0.33 and 1. An assumed skill difference in acquiring single targets leads to considerable differences in payoff at high FST. The estimated

payoff at (-30%; 30%) skill difference qualitatively corresponds to the observed payoff difference range (*cf.* Fig. 7a). Already for small skill differences (above 6%), a competitive FST=1 strategy becomes optimal for the participant with superior skill (Fig. 7c). For the less skilled participant, the optimal FST is around 1/3 (see Fig. S5b). The greater the skill difference, the more the individual participants' optimal strategies deviate from each other (Fig. 7c).

This analysis begs the question of how far the chosen strategy of each participant, i.e. their level of cooperation vs competition, deviates from the optimal given their skill. In particular, higher-skilled participants who chose cooperation could have increased their payoffs if they had chosen a competitive approach. Note that it only makes sense to consider the options of the higher-skilled participants because only they can make a profitable unilateral decision to pursue single targets competitively instead of cooperation. To quantify the loss of payoff (the cost of cooperation) due to a suboptimal individual strategy, we estimate the skill difference within the dyad, independent of FST. For that purpose, we use the normalized single target collection difference during single target acquisitions with straight trajectories, where we assume that both agents competed for the single target. Under this measure of skill difference, we can extrapolate the expected payoff to other FST values. For each dyad, we calculate the loss of payoff as compared to the optimal FST=1 scenario (Fig. 7d). For the higher-skilled participants, the cost of cooperation can be as high as 7 €.

Overall, these results demonstrate that many participants do not follow their individually-optimal strategies. All participants in the highly cooperative dyads at FST=0 are suboptimal independently of their potential skill differences. That includes the lower-skilled participants, who would also benefit from increasing the amount of single target to around FST=1/3 (Fig. S5b). The intermediate dyads around FST=1/3 are around the estimated optimum for the lower-skilled participant. Here the higher-skilled participants could simply increase the FST to exploit their optimal competitive strategy. Instead, however, they choose a more prosocial cooperative strategy. Interestingly, we did not observe a correlation between the skill difference within the dyad, and whether the dyad chose to follow a competitive or cooperative strategy (Fig. S5a). This suggests that factors beyond the selfish monetary gains of the higher-skilled participant influence the choice of the final strategy.

In summary, our findings demonstrate the interplay between skill differences within dyads and the optimal trade-off between cooperation and competition. As skill disparities increase, the individually optimal strategies of participants diverge, with higher-skilled participants benefiting from competitive strategies and lower-skilled participants profiting more from intermediate strategies. Despite these differences, many dyads chose to incur a cost of cooperation, favoring more prosocial strategies over maximizing their economic gain. This deviation from the optimal strategies underscores the complexity of decision-making in social settings, where factors beyond individual reward and effort, such as prosocial preferences or adherence to previously established cooperation, influence behavior.

Discussion

Historically, interaction experiments have been conducted using social dilemmas from game theory in a rigorous context but discrete in time and space. Compared to such discrete decisions, a tighter integration of continuous decisions with physical effectors such as eyes and limbs makes them more susceptible to sensorimotor affordances, as actions are not only planned but are iteratively recalibrated through direct sensory feedback [39, 45, 71]. Recent paradigms adopted more continuous approaches that resemble real-world decision-making [19, 27, 35, 39]. Prior work already leveraged cooperative [23, 28, 72], as well as competitive interactions [31, 32, 73, 74], into continuous action spaces. Similarly, in our foraging experiment participants could directly observe and react to their partner's ongoing decisions, embedding the interaction within embodied, real-time sensorimotor flow. The face-to-face arrangement and spatial continuity between collection cycles provided an additional layer of naturalism.

However, this transition towards continuity happens not only on the level of action spaces but also on the type of social interaction. While typical experiments offer only a fixed social context — either a cooperative, a competitive, or at most a binary dichotomy between these two — recent work by Pisauro and colleagues has began to investigate the continuous trade-off

between these extremes along a 1D axis [16]. In this Continuous Dilemma study, the shifts from cooperation to competition were elicited experimentally by the change of payoff formulation. Our work extends this novel line of research by combining direct action visibility within a continuous 2D action space with the opportunity for manifesting graded, spatially-dependent cooperative, intermediate, or competitive strategies under the same, "neutral" — if actual spatiotemporal contingencies are ignored — social context.

Conceptually, our paradigm synthesizes ideas from classical games such as Stag Hunt (coordination required to collect joint targets), Battle of the Sexes / Bach or Stravinsky (asymmetry of coordination options), and Prisoner's Dilemmas (choice between cooperation and competition), transferring them onto a continuous spatiotemporal interaction in a two-dimensional action space. Using this foraging paradigm, we recorded over 40 hours of continuous dyadic interactions that spanned the entire cooperation–competition spectrum. Strategies emerged not only at the extremes of pure cooperation and competition but also within a range of intermediate strategies. Our analysis indicates that travel path minimization underlies the emergence of this intermediate group. Generalizing this path minimization, by weighting target types based on stable cooperative or competitive tendencies in each dyad, we successfully characterized the large part of emergent strategies. Extending our model by recent interaction history and invite placements (sensorimotor communication) [70, 75–78] across collection cycles further enhanced prediction accuracy. Due to spatial continuity between cycles, a non-engaged participant can signal their intention to cooperate by inviting the partner to select a specific joint target. As hypothesized, the prediction improvement was more apparent in cooperative dyads compared to predominately competitive ones. However, contrary to our initial expectations, the effect was even stronger in the intermediate group. Thus particularly within the intermediate group, where decisions are made under constant tension between cooperative and competitive dynamics, the generation and integration of social information are increased. We speculate that invitations, especially the "active invitations" that take place after both participants tried to collect the single target, serve to relieve the social pressure after the competitive episode.

Linking across-cycle dynamics to within-cycle effects, we demonstrated that target choice uncertainty significantly shapes ensuing spatiotemporal interactions, leading to either mutually coupled sensorimotor dynamics or miscoordination when social information is unavailable and uncertainty is high [39, 73]. By quantifying the utility of sensorimotor communication as a reduction in target choice uncertainty, we found that intermediate dyads effectively leveraged this signal to arbitrate between cooperative and competitive strategies. The emergence and strategic use of sensorimotor communication for coordination are key outcomes of our continuous game design [77, 79, 80], distinguishing it from traditional discrete paradigms. These findings directly address the open question of how, and in which interactive scenarios, the sensorimotor communication arises, demonstrating that continuous, adaptive interactions are crucial for its emergence [70].

Since each collection cycle ends with the selection of one of three targets, it might seem that, similar to discrete mixed-motive games, decisions in our paradigm are reduced to a binary — or trinary, if the type of joint target is considered — choice between cooperation and competition. From this perspective, the gradual ratio of cooperation and competition is achieved only across multiple interactions. However, we argue that, unlike discrete paradigms, decisions in our task are shaped by a varying context determined by distances to targets and the partner. For instance, choosing a distant joint target over a nearby single target reflects a higher degree of cooperation than selecting a very close joint target. Additionally, classification can sometimes be misleading — e.g., participants may attempt to converge on a joint target but fail to coordinate, ultimately leading to a single target collection. In such cases, despite the final competitive outcome, the underlying interaction was mostly cooperative. Thus, in our paradigm varying levels of cooperation and competition can manifest not only across multiple but also within each cycle.

Our dyadic foraging game differs from classical foraging paradigms, which typically focus on the trade-off between exploiting the current resource and exploring new options under constraints of depleting rewards and the cost of exploration [81–83]. In our task, the only limited resource is the finite duration of the session, meaning that participants are not balancing

exploitation versus exploration but instead adapting their collection strategies within clearly defined, stable economic yet potentially volatile social context. Despite this difference, our paradigm is grounded in fundamental principles of foraging, as participants must dynamically allocate effort and make decisions under uncertainty — which arises not from environmental variability but from partly unpredictable actions of their partner. The sequential nature of decisions under spatiotemporal continuity creates a setting where distinct cooperative and competitive strategies emerge spontaneously, making this an ecologically valid variation of foraging in shared resource environments [84].

Analyzing the payoff efficiency showed that many participants did not adhere to their individual optimal strategy. Our analysis revealed two variables shaping the payoff function along the cooperation–competition spectrum unique to continuous action spaces: (i) the effect of an increase in movement speed for higher degrees of competition, associated with increased payoffs, and (ii) within-dyad sensorimotor skill differences. These factors are omnipresent in real-world scenarios and other continuous action spaces [31, 44], yet they are not captured in discrete (in time or in space) experiments. Beyond a competitive advantage, higher movement speeds towards single targets might reflect higher motivation when foraging for oneself [85, 86]. At the same time, our analysis highlights the critical role of skill differences, since they determine the optimal balance between cooperation and competition, both within our task and presumably across other continuous action spaces. But despite the opportunity for more skilled participants to maximize their individual payoff in a selfish manner, many adhered to overly cooperative strategies, paying a cost of cooperation.

The reluctance to exploit more competitive strategies, even when they are optimal, is likely an interplay of multiple factors. It might be explained by prosocial tendencies, characterized by empathy and a preference for fairness and reciprocity [87–89], as well as social norms [90–92]. In addition, once spontaneously established, social conventions may act as a stabilizing force, encouraging participants to adhere to a certain level of cooperation to maintain predictability and successful coordination [28, 93, 94]. The stabilizing effect of continuous transparent co-action is in line with continuous-time models of cooperation, which show how the propensity of agents to initiate cooperation and to mirror their partner's actions stabilizes at an evolutionary equilibrium [19]. Cooperation may also be a pragmatic strategy to reduce both physical and cognitive load. As in real foraging or hunting, participants might prioritize strategies that require less rapid, energy-intensive movements, thereby valuing comfort and sustainability over competitive optimization in a long experiment. Many dyads, especially the three fully cooperative turn-taking dyads, alternated between the joint targets, minimizing decision complexity [95]. Lastly, successful cooperation might be less stress-inducing or more rewarding, and thereby subjectively more appealing than competition [96].

Cooperative tendencies in our study might be further amplified by the face-to-face visibility and the transparency of action consequences [19, 27]. Even though the actual interaction took place on the abstract game field between the two virtual agents, the presence and direct visibility of a real partner has likely increased social salience [97]. Indeed, it has been demonstrated that dynamic reciprocity is abolished when participants believe that they interact with a computer agent [98]. At the same time, the attribution of agency and intentions to movements of virtual agents [99, 100] was, in addition to our results, apparent in the emotional reaction of viewers to gameplay sequences (to experience this firsthand, we encourage readers to view the gameplay videos: Supplementary Movies).

When watching the gameplay movies, the remarkable behavioral complexity of continuous spatiotemporal interactions and mutual coupling between agents become very apparent. Therefore, the transition towards studying continuous decisions requires not only the development of tasks that capture the range of archetypal interactions, but also sophisticated analysis techniques [39, 58]. Despite the strategic diversity, we successfully modeled a large part of the observed interactions and characterized the inherent links between target choice uncertainty, trajectories, and the underlying continuous decision processes. The trajectories, however, clearly provide more information about the continuous decision processes than could be captured by our modeling approach. Due to game continuity and action transparency mediating

mutually coupled interactions, we observed many high curvature trajectories reflecting miscoordination, indecision, changes of mind or online adjustments to partner's actions. Models that approximate the continuity of the spatiotemporal trajectories more closely, i.e. by predicting actual spatiotemporal dynamics that incorporate ongoing mutual coupling, represent a promising research direction. To make the game even more real-world-like and elicit richer dynamics, future experiments might manipulate the ambiguity of information about the targets and the partner actions, or make the landscape non-uniform in terms of effort and reward probability [16, 58]. These adaptations also offer an opportunity to infer the decision points in a large number of interactions, which could serve as salient alignment points for the neural analysis of continuous decisions [44, 47, 58, 101].

Our analysis of continuous decisions along the cooperation–competition spectrum yields valuable insights for the design of future experiments. First, it emphasizes the importance of factoring in the effect of increased movement speed during competitive behavior when formulating the payoff. While we successfully demonstrated that participants performed overly cooperative strategies that incur an associated cost of cooperation, our "flat" payoff formulation did not allow manifesting strategies that are overly competitive and result in a "cost of competition". This is because we did not anticipate, and hence did not compensate for the increase in speed during competition in our payoff formulation. By decreasing the payoff for single targets, we hypothesize that manifestations and quantification of such overly competitive strategies will become possible. The second insight is that the within-dyad skill difference determines the optimal trade-off between cooperation and competition. We successfully developed a skill difference measure to estimate the cost of cooperation for intermediate dyads, but for highly cooperative dyads (FST < 0.1) we could only estimate a lower bound due to limited skill difference data. To address this in future work, an additional measurement of skill differences closely aligned with the task should provide a more comprehensive estimate of the cost of cooperation.

Finally, while we can reliably predict stable decision-making, it remains unknown what causes the broad strategic diversity in the first place. This raises the question of whether the convergence to a specific strategy in each dyad is a consequence of (i) few initial spatial configurations that strongly shape the ensuing interactions (akin to a complex system evolving towards an attractor), (ii) a specific combination of personality predispositions of the two participants [102–105], or (iii) an interplay of both factors. Future research should explore these possibilities by systematically manipulating initial conditions, assessing personality traits, and leveraging computational modeling to disentangle their relative contributions to strategic convergence.

In summary, we contribute to the growing field of continuous decisions by developing a novel, richly flexible but tractable paradigm that affords cooperative and cooperative strategies within the same social context, under conditions of direct action visibility. Our analysis reveals the spontaneous emergence of stable strategies, spanning from cooperation to intermediate strategies to pure competition. The model incorporating weighted path minimization and across-cycle dynamics demonstrates that dyads with intermediate strategy rely on sensorimotor communication to facilitate coordination between cooperation and competition. We show that preceding interactions together with the initial conditions at the start of each collection cycle shape the decision uncertainty and within-cycle spatiotemporal dynamics, ultimately giving rise to specific target choices. These results form a solid basis for future research aimed at identifying where and how these factors are represented in the brain and exploring the interplay between different strategies, individual personality traits, and social contexts.

Methods

Participants

124 adult human participants participated in the study as paid volunteers. All participants gave written informed consent for participation after the procedures had been explained to them and before taking part in the experiment. Experiments were performed in accordance with institutional guidelines for experiments with humans and adhered to the principles of the

Declaration of Helsinki. The experimental protocol was approved by the ethics committee of the Georg-Elias-Mueller-Institute for Psychology, University of Goettingen (GEMI 17-06-06 171). Participants were tested in pairs as 62 unique dyads, i.e., each participant contributed only once. 4 dyads were excluded from the current analysis because they exhibited large differences in behavior between blocks. The analyzed dataset included 116 participants in 58 dyads (19 females, mean ± SD age: 25 ± 4 years, range 18–36 years, 5 mixed female/male dyads). Most participants were male because they were recruited for a related ongoing study of male hormonal effects.

Experimental procedures

Pairs of participants (dyads) played the Cooperation–Competition Foraging game, sitting face-to-face across the table (120-140 cm inter-subject distance) with a large transparent screen in between (Eyevis 55" OLED, 1920×1080 pixels, 60 Hz refresh rate, Movie S1, YouTube, OSF) [24, 106]. The visual stimuli presented on the screen were visible from both sides. The task was implemented in Python 3.10 and run on Ubuntu 20.04 LTS. Prior to the experiment, participants received written instructions detailing the game mechanics, the payoff structure for each target type, and the the procedure for determining their earnings (see Supplementary Information, Instructions for participants). Verbal clarifications were provided as needed to ensure full comprehension. In particular, participants were explicitly informed that their earnings would be performance-based, reflecting their cumulative payoffs during one randomly selected game block. Each experimental session consisted of two game blocks, each lasting 20 minutes. Participants were given breaks between blocks to minimize fatigue. Participants were not allowed to talk. At the end of the session, participants rolled a die to randomly determine which block's accumulated payoff would serve as their actual earnings.

The Cooperation–Competition Foraging game

The objective in the dyadic cooperation–competition foraging game is to earn money by collecting targets. To collect a target, participants were required to hover with their mouse-controlled cursors ("agents", blue and orange smaller circles, 2 cm diameter, 1.9 degrees of visual angle [°]) at 60 cm viewing distance) over the selected target (a bigger circle, 5 cm diameter, 4.8°) for one second. At any given time, the game field (a square with 51 cm side, 56°, with visible borders) contained three targets: one single target and two joint targets. All targets and agents were visible to both participants and were positioned randomly at the start of block session using the 2D uniform distribution. After target collection (end of collection cycle), the target of the same type immediately reappeared at a new random position, with no restrictions on reappearing near previous position. The positions of both agents and the two uncollected targets are not reset, ensuring a continuous transition between successive collection cycles.

The single target, which was white, could be collected by one participant alone ("winner-takes-all"). When an agent entered a single target, its color changed to match the agent's color, signaling whose agent was first and which participant would receive the payoff of 0.07€. The other participant received no payoff. Joint targets, which were partly blue, partly orange, required both participants to hover their agents over the target simultaneously to initiate the collection period. The color of joint target sectors reflected the asymmetric payoff distribution: one type offered 0.05€ to the blue agent and 0.02€ to the orange agent, and vice versa. The accumulated payoff of each participant was continuously shown in the lower right corner of the game field.

During target collection, a transparent disk expanded from the center to the edge of the target, visually indicating collection progress. Auditory feedback was provided through a sound with a continuously increasing pitch. If a participant left the target before the collection was complete, the progress was reset, and an error sound was played. Successful collection was confirmed by the target's disappearance and a short reward-associated sound.

To reduce the dependence of motor skill and to reflect the spatiotemporal limitations of realistic foraging, a maximum agent speed was set to to 42.6 cm/s. If a participant exceeded this maximum, their agent lagged relative to the mouse input. To ensure high temporal precision for the movement data, agents' positions were tracked at a sampling rate of 120 Hz.

Timecourse of strategies over an experimental session

For the analysis of the stationarity of the strategies over an experimental session, we calculated the moving average of the fraction of single targets (FST) collected by both agents in dyad during a moving window of 1 minute for the analysis in Fig. 2, and 30 seconds for the analysis in Fig. 4.

Generalized Linear Model (GLM) for dyadic target choice

Our modeling allows us to analyze which factors determine the target choice of the dyad. Specifically, we predicted the collected target identity from the position of the two agents at the beginning of the collection cycle, the position of the targets, and potentially from the outcomes of the previous cycle. For the distance weighting GLM, the predicted target is the one with the weighted minimal potential distance to acquire a target j (with j being either the single target, the joint target benefiting player A or the joint target benefiting player B):

$$j_{\text{pred}} = \text{argmin}_j \left[D_S \left(1 - w\right), D_{J,A} \cdot w, D_{J,B} \cdot w \right]_j , \tag{1}$$

where D_S is the minimal distance from the single target to either agent, $D_{J,A}$ (or $D_{J,B}$) is the maximal distance between the joint target benefiting agent A (B) to either agent and w a weighting factor such that the observed FST (fraction of single targets) is reached (for details, see Supplementary Methods 1.1).

This model was also used to simulate the optimal strategy for the dyad. For the range of possible weighting factors, we ran simulations of the game, where the choice of the target was given by the weighted distance formula above. We ran two different simulations: the agents either moved simultaneously or, when collecting a single target, the non-collecting agent placed himself on the game field such that the subsequent expected acquisition time is minimal (called "advantageous placement", see Supplementary Methods 1.1 and Fig. 3c).

For the full GLM, we framed our model as a multiclass classification problem. We predicted the probability of observing the collection of each of the three targets given the vector $\vec{x}$, that is the distances to the targets, the identities of targets collected in previous cycles, and whether an "invitation" is present in the current cycle (the non-collecting agent is near a joint target):

$$P(j_{\text{obs}} = j|\vec{x}) = \text{Softmax}\left(\boldsymbol{\theta}^T \cdot \vec{x}\right)_j . \tag{2}$$

We took certain symmetries of the problems into account, mainly that the identity of both players are interchangeable, to reduce the number of parameters to be estimated (see Supplementary Methods 1.2). The regression coefficients $\boldsymbol{\theta}$ were estimated by minimizing the loss with the Broyden–Fletcher–Goldfarb–Shanno (BFGS) algorithm. To avoid overfitting and for estimating the accuracy of the model, we used 5-fold cross-validation.

To obtain a quantification of the certainty of the choice of the dyad, we measured the entropy H of the target prediction:

$$H = -\sum_{j=1}^{3} P(j_{\text{obs}} = j|\vec{x}) \cdot \log_2 \left(P(j_{\text{obs}} = j|\vec{x})\right) . \tag{3}$$

Trajectory classification

To characterize the ongoing decision process during the acquisition period, we classified movement trajectories based on their shape relative to the targets, into six categories — "invitation", "failed invitation", "strongly curved", "different targets", "one ahead" and "concurrent" — using a set of heuristic rules for each category applied in that specific order. If the trajectory followed the rule, the trajectory was classified as such, if not, the next rule was tried. For precise definitions, see Supplementary Methods 1.3.

Disentangling of spatiotemporal factors shaping the payoff

To understand how trajectory efficiency, speed, and positioning influence agents' payoffs, we disentangled these different factors. We expressed the payoff as an addition/subtraction of the different factors that determine the trajectory length, divided by the mean speed, to obtain the contribution of each factor to the total joint payoff for each dyad. This decomposition is not exact: estimating the average payoff per cycle using the average trajectory length and mean speed introduces a small error, since the average of a ratio is not strictly equal to the ratio of averages. However, in this case, the correlation is nearly perfect ($r = 0.99$, see also Supplementary Methods 1.4).

Skill difference estimation

The skill difference between participants influences how successful an agent is in competing for single targets. This is also the approach we used to effectively estimate the skill difference, by measuring the fraction of single targets each agent manages to collect. Thus, we could not estimate the skill difference if the agents always played cooperatively. To calculate the skill difference, we did not take into account cycles where the participants did not compete for the same target, by excluding the classes "Different targets" and "Failed invitations" (see Supplementary Methods 1.5 and 1.6).

Estimating of the cost of cooperation from counterfactual scenarios

To obtain an estimate of the cost of cooperation, i.e. an estimation of what would have happened if dyads had played more competitively than observed, we built a model that allows us to counterfactually estimate the payoff for other values of the FST Φ than observed for the dyad in question. Specifically, we estimated the payoff $\hat{R}^X(\Phi)$ of each agent X by combining an estimate of the average joint payoff $\hat{R}(\Phi)$ with an estimate of the difference of payoff between the two agents in a dyad $\hat{R}^X_\Delta(\Phi)$ (see Supplementary Methods 1.6). The estimate of the average joint payoff was obtained by fitting the variables that shape the payoff, the average distance between target collections, the average reduction of this distance due to an advantageous placement, the average increase of distance due to trajectory curvature, and the average agent speed over all dyads. The difference of payoff between agents was estimated per dyad individually and is dependent on the skill difference of the participants. Thus, with this estimation of the dependence of the payoff on the FST, we could obtain the payoff increase if the participants had played more competitively.

Statistical analyses

All statistical tests were two-sided. For the Mann-Whitney U tests and paired Wilcoxon signed-rank tests, the median (Mdn) followed by the interquartile range (IQR: [quartile 1, quartile 3]) for each group or condition is reported; the effect size r_{rb} was measured by the rank biserial correlation, and 95% confidence intervals (CI) for the effect size are provided. For the binomial tests, Clopper-Pearson exact method for the 95% confidence intervals of the proportion was used. Pearson's product moment correlation coefficient r and its 95% CI are used to report correlations.

To calculate the statistical significance of the coefficients of the GLM in each dyad, we used the Wald test and estimated the required variance matrix by inverting the Hessian matrix at the maximum likelihood estimate [107]. The resulting p-values were adjusted for multiple comparisons (N=58) to control the false discovery rate using Benjamini-Hochberg procedure.

Statistical tests were calculated in R version 4.4.2 and in Python 3.10.

References

[1] C. D. Frith and D. M. Wolpert, eds. *The Neuroscience of Social Interaction: Decoding, Influencing, and Imitating the Actions of Others*. 2004.

[2] M. Stallen and A. G. Sanfey. "The cooperative brain". *The Neuroscientist* 19.3 (2013), pp. 292–303.

[3] R. Báez-Mendoza, E. P. Mastrobattista, A. J. Wang, and Z. M. Williams. "Social agent identity cells in the prefrontal cortex of interacting groups of primates". *Science* 374.6566 (2021), eabb4149. DOI: 10.1126/science.abb4149.

[4] H. Wang and A. C. Kwan. "Competitive and cooperative games for probing the neural basis of social decision-making in animals". *Neuroscience & Biobehavioral Reviews* 149 (2023), p. 105158. DOI: 10.1016/j.neubiorev.2023.105158.

[5] A. G. Sanfey. "Social Decision-Making: Insights from Game Theory and Neuroscience". *Science* 318.5850 (2007), pp. 598–602. DOI: 10.1126/science.1142996.

[6] J. K. Rilling, B. King-Casas, and A. G. Sanfey. "The neurobiology of social decision-making". *Current Opinion in Neurobiology* 18.2 (2008), pp. 159–165. DOI: 10.1016/j.conb.2008.06.003.

[7] C. C. Ruff and E. Fehr. "The neurobiology of rewards and values in social decision making". *Nature Reviews Neuroscience* 15.8 (2014), pp. 549–562. DOI: 10.1038/nrn3776.

[8] A. G. Sanfey, C. Civai, and P. Vavra. "Predicting the other in cooperative interactions". *Trends in Cognitive Sciences* 19.7 (2015), pp. 364–365. DOI: 10.1016/j.tics.2015.05.009.

[9] S. W. C. Chang. "An Emerging Field of Primate Social Neurophysiology: Current Developments". *eNeuro* 4.5 (2017), ENEURO.0295–17.2017. DOI: 10.1523/ENEURO.0295-17.2017.

[10] M. K. Wittmann, P. L. Lockwood, and M. F. Rushworth. "Neural Mechanisms of Social Cognition in Primates". *Annual Review of Neuroscience* 41.1 (2018), pp. 99–118. DOI: 10.1146/annurev-neuro-080317-061450.

[11] R. Philippe, R. Janet, K. Khalvati, R. P. N. Rao, D. Lee, and J.-C. Dreher. "Neurocomputational mechanisms involved in adaptation to fluctuating intentions of others". *Nature Communications* 15.1 (2024), p. 3189. DOI: 10.1038/s41467-024-47491-2.

[12] D. Lee. "Game theory and neural basis of social decision making". *Nature Neuroscience* 11.4 (2008), pp. 404–409. DOI: 10.1038/nn2065.

[13] J. M. van Baar, L. J. Chang, and A. G. Sanfey. "The computational and neural substrates of moral strategies in social decision-making". *Nature Communications* 10.1 (2019), p. 1483. DOI: 10.1038/s41467-019-09161-6.

[14] A. Peysakhovich, M. A. Nowak, and D. G. Rand. "Humans display a 'cooperative phenotype' that is domain general and temporally stable". *Nature Communications* 5.1 (2014), p. 4939. DOI: 10.1038/ncomms5939.

[15] S. Le and R. Boyd. "Evolutionary dynamics of the continuous iterated Prisoner's dilemma". *Journal of Theoretical Biology* 245.2 (2007), pp. 258–267. DOI: 10.1016/j.jtbi.2006.09.016.

[16] M. A. Pisauro, E. F. Fouragnan, D. H. Arabadzhiyska, M. a. J. Apps, and M. G. Philiastides. "Neural implementation of computational mechanisms underlying the continuous trade-off between cooperation and competition". *Nature Communications* 13.1 (2022), p. 6873. DOI: 10.1038/s41467-022-34509-w.

[17] L. A. Dugatkin, M. Mesterton-Gibbonsand, and A. I. Houston. "Beyond the prisoner's dilemma: Toward models to discriminate among mechanisms of cooperation in nature". *Trends in Ecology & Evolution* 7.6 (1992), pp. 202–205. DOI: 10.1016/0169-5347(92)90074-L.

[18] R. Noë. "Cooperation experiments: coordination through communication versus acting apart together". *Animal Behaviour* 71.1 (2006), pp. 1–18. DOI: 10.1016/j.anbehav.2005.03.037.

[19] G. S. van Doorn, T. Riebli, and M. Taborsky. "Coaction versus reciprocity in continuous-time models of cooperation". *Journal of Theoretical Biology* 356 (2014), pp. 1–10. DOI: 10.1016/j.jtbi.2014.03.019.

[20] S. F. Brosnan, L. Salwiczek, and R. Bshary. "The interplay of cognition and cooperation". *Philosophical Transactions of the Royal Society B: Biological Sciences* 365.1553 (2010), pp. 2699–2710. DOI: 10.1098/rstb.2010.0154.

[21] S. F. Brosnan, B. J. Wilson, and M. J. Beran. "Old World monkeys are more similar to humans than New World monkeys when playing a coordination game". *Proceedings. Biological Sciences* 279.1733 (2012), pp. 1522–1530. DOI: 10.1098/rspb.2011.1781.

[22] S. F. Brosnan, S. A. Price, K. Leverett, L. Prétôt, M. Beran, and B. J. Wilson. "Human and monkey responses in a symmetric game of conflict with asymmetric equilibria". *Journal of Economic Behavior & Organization* 142 (2017), pp. 293–306. DOI: 10.1016/j.jebo.2017.07.037.

[23] W. S. Ong, S. Madlon-Kay, and M. L. Platt. "Neuronal correlates of strategic cooperation in monkeys". *Nature Neuroscience* 24.1 (2021), pp. 116–128. DOI: 10.1038/s41593-020-00746-9.

[24] S. Moeller, A. M. Unakafov, J. Fischer, A. Gail, S. Treue, and I. Kagan. "Human and macaque pairs employ different coordination strategies in a transparent decision game". *eLife* 12 (2023), e81641. DOI: 10.7554/eLife.81641.

[25] A. Formaux, D. Paleressompoulle, J. Fagot, and N. Claidière. "The experimental emergence of convention in a non-human primate". *Philosophical Transactions of the Royal Society B: Biological Sciences* 377.1843 (2022), p. 20200310. DOI: 10.1098/rstb.2020.0310.

[26] A. M. Unakafov, T. Schultze, A. Gail, S. Moeller, I. Kagan, S. Eule, and F. Wolf. "Emergence and suppression of cooperation by action visibility in transparent games". *PLOS Computational Biology* 16.1 (2020), e1007588. DOI: 10.1371/journal.pcbi.1007588.

[27] D. Friedman and R. Oprea. "A Continuous Dilemma". *American Economic Review* 102.1 (2012), pp. 337–363. DOI: 10.1257/aer.102.1.337.

[28] R. X. D. Hawkins and R. L. Goldstone. "The Formation of Social Conventions in Real-Time Environments". *PLOS ONE* 11.3 (2016), e0151670. DOI: 10.1371/journal.pone.0151670.

[29] S. S. Wiltermuth and C. Heath. "Synchrony and Cooperation". *Psychological Science* 20.1 (2009), pp. 1–5. DOI: 10.1111/j.1467-9280.2008.02253.x.

[30] S. N. Iqbal, L. Yin, C. B. Drucker, Q. Kuang, J.-F. Gariépy, M. L. Platt, and J. M. Pearson. "Latent goal models for dynamic strategic interaction". *PLOS Computational Biology* 15.3 (2019), e1006895. DOI: 10.1371/journal.pcbi.1006895.

[31] K. R. McDonald, W. F. Broderick, S. A. Huettel, and J. M. Pearson. "Bayesian nonparametric models characterize instantaneous strategies in a competitive dynamic game". *Nature Communications* 10.1 (2019), p. 1808. DOI: 10.1038/s41467-019-09789-4.

[32] S. B. M. Yoo, J. C. Tu, S. T. Piantadosi, and B. Y. Hayden. "The neural basis of predictive pursuit". *Nature Neuroscience* 23.2 (2020), pp. 252–259. DOI: 10.1038/s41593-019-0561-6.

[33] J. M. van Baar, F. H. Klaassen, F. Ricci, L. J. Chang, and A. G. Sanfey. "Stable distribution of reciprocity motives in a population". *Scientific Reports* 10.1 (2020), p. 18164. DOI: 10.1038/s41598-020-74818-y.

[34] N. Sebanz and G. Knoblich. "Progress in Joint-Action Research". *Current Directions in Psychological Science* 30.2 (2021), pp. 138–143. DOI: 10.1177/0963721420984425.

[35] S. Fan, O. D. Monte, and S. W. Chang. "Levels of Naturalism in Social Neuroscience Research". *iScience* (2021), p. 102702. DOI: 10.1016/j.isci.2021.102702.

[36] L. V. Hadley, G. Naylor, and A. F. d. C. Hamilton. "A review of theories and methods in the science of face-to-face social interaction". *Nature Reviews Psychology* 1.1 (2022), pp. 42–54. DOI: 10.1038/s44159-021-00008-w.

[37] A. F. d. C. Hamilton and J. Holler. "Face2face: advancing the science of social interaction". *Philosophical Transactions of the Royal Society B: Biological Sciences* 378.1875 (2023), p. 20210470. DOI: 10.1098/rstb.2021.0470.

[38] N. Coucke, M. K. Heinrich, M. Dorigo, and A. Cleeremans. "Action-based confidence sharing and collective decision making". *iScience* 27.10 (2024), p. 111006. DOI: 10.1016/j.isci.2024.111006.

[39] S. B. M. Yoo, B. Y. Hayden, and J. M. Pearson. "Continuous decisions". *Philosophical Transactions of the Royal Society of London. Series B, Biological Sciences* 376.1819 (2021), p. 20190664. DOI: 10.1098/rstb.2019.0664.

[40] P. Cisek and J. F. Kalaska. "Neural Mechanisms for Interacting with a World Full of Action Choices". *Annu Rev Neurosci* (2010). DOI: 10.1146/annurev.neuro.051508.135409.

[41] D. M. Wolpert, K. Doya, and M. Kawato. "A unifying computational framework for motor control and social interaction". *Philosophical Transactions of the Royal Society of London. Series B: Biological Sciences* 358.1431 (2003), pp. 593–602. DOI: 10.1098/rstb.2002.1238.

[42] D. A. Braun, P. A. Ortega, and D. M. Wolpert. "Nash Equilibria in Multi-Agent Motor Interactions". *PLOS Computational Biology* 5.8 (2009), e1000468. DOI: 10.1371/journal.pcbi.1000468.

[43] J. P. Gallivan, L. Logan, D. M. Wolpert, and J. R. Flanagan. "Parallel specification of competing sensorimotor control policies for alternative action options". *Nature Neuroscience* 19.2 (2016), pp. 320–326. DOI: 10.1038/nn.4214.

[44] J. P. Gallivan, C. S. Chapman, D. M. Wolpert, and J. R. Flanagan. "Decision-making in sensorimotor control". *Nature Reviews Neuroscience* 19.9 (2018), pp. 519–534. DOI: 10.1038/s41583-018-0045-9.

[45] P. Cisek. "Making decisions through a distributed consensus". *Current Opinion in Neurobiology* 22.6 (2012), pp. 927–936. DOI: 10.1016/j.conb.2012.05.007.

[46] J. Michalski, A. M. Green, and P. Cisek. "Reaching decisions during ongoing movements". *Journal of Neurophysiology* 123.3 (2020), pp. 1090–1102. DOI: 10.1152/jn.00613.2019.

[47] P. Ulbrich and A. Gail. "Deciding While Acting—Mid-Movement Decisions Are More Strongly Affected by Action Probability than Reward Amount". *eNeuro* 10.4 (2023). DOI: 10.1523/ENEURO.0240-22.2023.

[48] C. Lindig-León, G. Schmid, and D. A. Braun. "Bounded rational response equilibria in human sensorimotor interactions". *Proceedings of the Royal Society B: Biological Sciences* 288.1962 (2021), p. 20212094. DOI: 10.1098/rspb.2021.2094.

[49] G. Pezzulo and P. Cisek. "Navigating the Affordance Landscape: Feedback Control as a Process Model of Behavior and Cognition". *Trends in Cognitive Sciences* 20.6 (2016), pp. 414–424. DOI: 10.1016/j.tics.2016.03.013.

[50] R. Shadmehr, H. J. Huang, and A. A. Ahmed. "A Representation of Effort in Decision-Making and Motor Control". *Current Biology* 26.14 (2016), pp. 1929–1934. DOI: 10.1016/j.cub.2016.05.065.

[51] P. Morel, P. Ulbrich, and A. Gail. "What makes a reach movement effortful? Physical effort discounting supports common minimization principles in decision making and motor control". *PLOS Biology* 15.6 (2017), e2001323. DOI: 10.1371/journal.pbio.2001323.

[52] D. W. Stephens and J. R. Krebs. *Foraging Theory*. Vol. 1. 1986. ISBN: 978-0-691-08441-1. DOI: 10.2307/j.ctvs32s6b.

[53] D. Mobbs, P. C. Trimmer, D. T. Blumstein, and P. Dayan. "Foraging for foundations in decision neuroscience: insights from ethology". *Nature Reviews Neuroscience* 19.7 (2018), pp. 419–427. DOI: 10.1038/s41583-018-0010-7.

[54] B. Y. Hayden, J. M. Pearson, and M. L. Platt. "Neuronal basis of sequential foraging decisions in a patchy environment". *Nature Neuroscience* 14.7 (2011), pp. 933–939. DOI: 10.1038/nn.2856.

[55] J. S. Diamond, D. M. Wolpert, and J. R. Flanagan. "Rapid target foraging with reach or gaze: The hand looks further ahead than the eye". *PLOS Computational Biology* 13.7 (2017). Ed. by A. A. Faisal, e1005504. DOI: 10.1371/journal.pcbi.1005504.

[56] T. Yoon, R. B. Geary, A. A. Ahmed, and R. Shadmehr. "Control of movement vigor and decision making during foraging". *Proceedings of the National Academy of Sciences* 115.44 (2018), E10476–E10485. DOI: 10.1073/pnas.1812979115.

[57] N. Shahidi, M. Franch, A. Parajuli, P. Schrater, A. Wright, X. Pitkow, and V. Dragoi. "Population coding of strategic variables during foraging in freely moving macaques". *Nature Neuroscience* 27.4 (2024), pp. 772–781. DOI: 10.1038/s41593-024-01575-w.

[58] P. Cisek and A. M. Green. "Toward a neuroscience of natural behavior". *Current Opinion in Neurobiology* 86 (2024), p. 102859. DOI: 10.1016/j.conb.2024.102859.

[59] J. Gordon, A. Maselli, G. L. Lancia, T. Thiery, P. Cisek, and G. Pezzulo. "The road towards understanding embodied decisions". *Neuroscience & Biobehavioral Reviews* 131 (2021), pp. 722–736. DOI: 10.1016/j.neubiorev.2021.09.034.

[60] K. Allen et al. "Using games to understand the mind". *Nature Human Behaviour* 8.6 (2024), pp. 1035–1043. DOI: 10.1038/s41562-024-01878-9.

[61] V. Simonelli, D. Nuzzi, G. L. Lancia, and G. Pezzulo. "Human foraging strategies flexibly adapt to resource distribution and time constraints" (2025). DOI: 10.48550/arXiv.2408.01350.

[62] Y. E. Wu and W. Hong. "Neural basis of prosocial behavior". *Trends in Neurosciences* 45.10 (2022), pp. 749–762. DOI: 10.1016/j.tins.2022.06.008.

[63] A. Soltani, J. D. Murray, H. Seo, and D. Lee. "Timescales of cognition in the brain". *Current Opinion in Behavioral Sciences*. Value based decision-making 41 (2021), pp. 30–37. DOI: 10.1016/j.cobeha.2021.03.003.

[64] M. E. Walton, S. W. Kennerley, D. M. Bannerman, P. E. M. Phillips, and M. F. S. Rushworth. "Weighing up the benefits of work: Behavioral and neural analyses of effort-related decision making". *Neural Networks* 19.8 (2006), pp. 1302–1314. DOI: 10.1016/j.neunet.2006.03.005.

[65] P. L. Croxson, M. E. Walton, J. X. O'Reilly, T. E. J. Behrens, and M. F. S. Rushworth. "Effort-Based Cost-Benefit Valuation and the Human Brain". *Journal of Neuroscience* 29.14 (2009), pp. 4531–4541. DOI: 10.1523/JNEUROSCI.4515-08.2009.

[66] V. Skvortsova, S. Palminteri, and M. Pessiglione. "Learning To Minimize Efforts versus Maximizing Rewards: Computational Principles and Neural Correlates". *Journal of Neuroscience* 34.47 (2014), pp. 15621–15630. DOI: 10.1523/JNEUROSCI.1350-14.2014.

[67] T. T.-J. Chong, M. Apps, K. Giehl, A. Sillence, L. L. Grima, and M. Husain. "Neurocomputational mechanisms underlying subjective valuation of effort costs". *PLOS Biology* 15.2 (2017), e1002598. DOI: 10.1371/journal.pbio.1002598.

[68] M. Burrell, A. Pastor-Bernier, and W. Schultz. "Worth the Work? Monkeys Discount Rewards by a Subjective Adapting Effort Cost". *J. Neurosci.* 43.40 (2023), pp. 6796–6806. DOI: 10.1523/JNEUROSCI.0115-23.2023.

[69] L. Suriya-Arunroj and A. Gail. "Complementary encoding of priors in monkey frontoparietal network supports a dual process of decision-making". *eLife* 8 (2019). Ed. by E. Vaadia and R. B. Ivry, e47581. DOI: 10.7554/eLife.47581.

[70] G. Pezzulo, F. Donnarumma, H. Dindo, A. D'Ausilio, I. Konvalinka, and C. Castelfranchi. "The body talks: Sensorimotor communication and its brain and kinematic signatures". *Physics of Life Reviews* 28 (2019), pp. 1–21. DOI: 10.1016/j.plrev.2018.06.014.

[71] P. Cisek and A. Pastor-Bernier. "On the challenges and mechanisms of embodied decisions". *Phil. Trans. R. Soc. B* 369.1655 (2014), p. 20130479. DOI: 10.1098/rstb.2013.0479.

[72] S. Ferrari-Toniolo, F. Visco-Comandini, and A. Battaglia-Mayer. "Two Brains in Action: Joint-Action Coding in the Primate Frontal Cortex". *Journal of Neuroscience* 39.18 (2019), pp. 3514–3528. DOI: 10.1523/JNEUROSCI.1512-18.2019.

[73] S. B. M. Yoo, J. C. Tu, and B. Y. Hayden. "Multicentric tracking of multiple agents by anterior cingulate cortex during pursuit and evasion". *Nature Communications* 12.1 (2021), p. 1985. DOI: 10.1038/s41467-021-22195-z.

[74] T. Hosokawa and M. Watanabe. "Prefrontal Neurons Represent Winning and Losing during Competitive Video Shooting Games between Monkeys". *Journal of Neuroscience* 32.22 (2012), pp. 7662–7671. DOI: 10.1523/JNEUROSCI.6479-11.2012.

[75] G. Pezzulo, F. Donnarumma, and H. Dindo. "Human Sensorimotor Communication: A Theory of Signaling in Online Social Interactions". *PLOS ONE* 8.11 (2013), e79876. DOI: 10.1371/journal.pone.0079876.

[76] L. McEllin and J. Michael. "Sensorimotor communication fosters trust and generosity: The role of effort and signal utility". *Cognition* 224 (2022), p. 105066. DOI: 10.1016/j.cognition.2022.105066.

[77] T. Buidze, T. Sommer, K. Zhao, X. Fu, and J. Gläscher. "Communication with Surprise – Computational and Neural Mechanisms for Non-Verbal Human Interactions". *bioRxiv* (2024). DOI: 10.1101/2024.02.20.581193.

[78] T. Buidze, T. Sommer, K. Zhao, X. Fu, and J. Gläscher. "Expectation violations signal goals in novel human communication". *Nature Communications* 16.1 (2025), p. 1989. DOI: 10.1038/s41467-025-57025-z.

[79] C. Vesper, L. Schmitz, L. Safra, N. Sebanz, and G. Knoblich. "The role of shared visual information for joint action coordination". *Cognition* 153.Supplement C (2016), pp. 118–123. DOI: 10.1016/j.cognition.2016.05.002.

[80] C. Vesper and V. Sevdalis. "Informing, Coordinating, and Performing: A Perspective on Functions of Sensorimotor Communication". *Frontiers in Human Neuroscience* 14 (2020), p. 168. DOI: 10.3389/fnhum.2020.00168.

[81] N. Kolling, T. E. J. Behrens, R. B. Mars, and M. F. S. Rushworth. "Neural Mechanisms of Foraging". *Science* 336.6077 (2012), pp. 95–98. DOI: 10.1126/science.1216930.

[82] B. Y. Hayden and M. E. Walton. "Neuroscience of foraging". *Frontiers in Neuroscience* 8 (2014). DOI: 10.3389/fnins.2014.00081.

[83] A. S. Gabay and M. A. J. Apps. "Foraging optimally in social neuroscience: computations and methodological considerations". *Social Cognitive and Affective Neuroscience* 16.8 (2021), pp. 782–794. DOI: 10.1093/scan/nsaa037.

[84] K. Garg, W. Deng, and D. Mobbs. "Beyond the individual: A social foraging framework to study decisions in groups" (2024). DOI: 10.31219/osf.io/rmqyb.

[85] P. L. Lockwood, M. Hamonet, S. H. Zhang, A. Ratnavel, F. U. Salmony, M. Husain, and M. A. J. Apps. "Prosocial apathy for helping others when effort is required". *Nature Human Behaviour* 1.7 (2017), pp. 1–10. DOI: 10.1038/s41562-017-0131.

[86] L. S. Contreras-Huerta, M. A. Pisauro, S. Küchenhoff, A. Gekiere, C. Le Heron, P. L. Lockwood, and M. A. J. Apps. "A reward self-bias leads to more optimal foraging for ourselves than others". *Scientific Reports* 14 (2024), p. 26845. DOI: 10.1038/s41598-024-69452-x.

[87] N. Eisenberg and P. Miller. "The Relation of Empathy to Prosocial and Related Behaviors". *Psychological bulletin* 101 (1987), pp. 91–119. DOI: 10.1037/0033-2909.101.1.91.

[88] J. K. Rilling, D. A. Gutman, T. R. Zeh, G. Pagnoni, G. S. Berns, and C. D. Kilts. "A Neural Basis for Social Cooperation". *Neuron* 35.2 (2002), pp. 395–405. DOI: 10.1016/S0896-6273(02)00755-9.

[89] S. Yamamoto and A. Takimoto. "Empathy and Fairness: Psychological Mechanisms for Eliciting and Maintaining Prosociality and Cooperation in Primates". *Social Justice Research* 25.3 (2012), pp. 233–255. DOI: 10.1007/s11211-012-0160-0.

[90] J. A. Flory, U. Gneezy, K. L. Leonard, and J. A. List. "Gender, age, and competition: A disappearing gap?" *Journal of Economic Behavior & Organization* 150 (2018), pp. 256–276. DOI: 10.1016/j.jebo.2018.03.027.

[91] L. Katz, L. Finestone, and D. M. Paskevich. "Competition when cooperation is the means to success: Understanding context and recognizing mutually beneficial situations". *Cogent Psychology* 8.1 (2021). Ed. by G. Prete, p. 1878984. DOI: 10.1080/23311908.2021.1878984.

[92] M. C. Madsen. "Developmental and Cross-Cultural Differences in the Cooperative and Competitive Behavior of Young Children". *Journal of Cross-Cultural Psychology* 2.4 (1971), pp. 365–371. DOI: 10.1177/002202217100200406.

[93] D. Centola and A. Baronchelli. "The spontaneous emergence of conventions: An experimental study of cultural evolution". *Proceedings of the National Academy of Sciences* 112.7 (2015), pp. 1989–1994. DOI: 10.1073/pnas.1418838112.

[94] M. Taborsky, J. G. Frommen, and C. Riehl. "Correlated pay-offs are key to cooperation". *Phil. Trans. R. Soc. B* 371.1687 (2016), p. 20150084. DOI: 10.1098/rstb.2015.0084.

[95] A. M. Colman and L. Browning. "Evolution of cooperative turn-taking". *Evolutionary Ecology Research* 11 (2009), pp. 949–963.

[96] M.-L. Halko and L. Sääksvuori. "Competitive behavior, stress, and gender". *Journal of Economic Behavior & Organization* 141 (2017), pp. 96–109. DOI: 10.1016/j.jebo.2017.06.014.

[97] B. Liefooghe, E. Min, and H. Aarts. "The effects of social presence on cooperative trust with algorithms". *Scientific Reports* 13.1 (2023), p. 17463. DOI: 10.1038/s41598-023-44354-6.

[98] A. Mahmoodi, B. Bahrami, and C. Mehring. "Reciprocity of social influence". *Nature Communications* 9.1 (2018), p. 2474. DOI: 10.1038/s41467-018-04925-y.

[99] F. Abell, F. Happé, and U. Frith. "Do triangles play tricks? Attribution of mental states to animated shapes in normal and abnormal development". *Cognitive Development* 15.1 (2000), pp. 1–16. DOI: 10.1016/S0885-2014(00)00014-9.

[100] F. Heider and M. Simmel. "An Experimental Study of Apparent Behavior". *The American Journal of Psychology* 57.2 (1944), pp. 243–259. DOI: 10.2307/1416950.

[101] P. Ulbrich and A. Gail. "The cone method: Inferring decision times from single-trial 3D movement trajectories in choice behavior". *Behavior Research Methods* 53.6 (2021), pp. 2456–2472. DOI: 10.3758/s13428-021-01579-5.

[102] K. Zhao and L. D. Smillie. "The Role of Interpersonal Traits in Social Decision Making: Exploring Sources of Behavioral Heterogeneity in Economic Games". *Personality and Social Psychology Review* 19.3 (2015), pp. 277–302. DOI: 10.1177/1088868314553709.

[103] E. Proto, A. Rustichini, and A. Sofianos. "Intelligence, Personality, and Gains from Cooperation in Repeated Interactions". *Journal of Political Economy* 127.3 (2019), pp. 1351–1390. DOI: 10.1086/701355.

[104] M. G. Edelson, R. Polania, C. C. Ruff, E. Fehr, and T. A. Hare. "Computational and neurobiological foundations of leadership decisions". *Science* 361.6401 (2018), eaat0036. DOI: 10.1126/science.aat0036.

[105] P. Faure, S. L. Fayad, C. Solié, and L. M. Reynolds. "Social Determinants of Inter-Individual Variability and Vulnerability: The Role of Dopamine". *Front. Behav. Neurosci.* 16 (2022). DOI: 10.3389/fnbeh.2022.836343.

[106] S. Isbaner, R. Báez-Mendoza, R. Bothe, A. Fischer, A. Gail, J. Gläscher, H. Lueschen, S. Moeller, S. Eiteljoerge, L. Penke, V. Priesemann, J. Ruß, A. Schacht, F. Schneider, N. Shahidi, S. Treue, M. Wibral, A. Ziereis, J. Fischer, I. Kagan, and N. Mani. *Dyadic Interaction Platform: A novel tool to study transparent social interactions.* 2025. DOI: 10.31234/osf.io/2rckn_v1.

[107] F. Tuerlinckx, F. Rijmen, G. Verbeke, and P. De Boeck. "Statistical inference in generalized linear mixed models: A review". *British Journal of Mathematical and Statistical Psychology* 59.2 (2006), pp. 225–255. DOI: 10.1348/000711005X79857.

Acknowledgments

We thank Dr. Sebastian Moeller and Klaus Heisig for the technical support with the Dyadic Interaction Platform, Dr. Annika Ziereis for helpful comments on the manuscript, Mariia Kadochnikova and Dr. Zahra Yousefi Darani for taking part in the game demonstration movie, and Karin Tilch and Thorge Beilfuß for the photos and the game demonstration movie, respectively. We thank Dr. Chris Schloegl for efficient scientific coordination of the Leibniz ScienceCampus Primate Cognition and the Collaborative Research Center SFB 1528 "Cognition of Interaction", and the members of these consortium for stimulating discussions.

Funding:

This work was supported by the Leibniz ScienceCampus Primate Cognition (to AG and IK), the Leibniz Collaborative Excellence grant K265/2019 "Neurophysiological mechanisms of primate interactions in dynamic sensorimotor settings" (to AG and IK), the Cluster of Excellence "Multiscale Bioimaging" (MBExC, to VP), and the German Research Foundation via the Collaborative Research Center "Cognition of Interaction" (DFG SFB-1528, projects A06, C02 and Z01, to LP, AS, AG, VP, and IK). The funders had no role in study design, data collection, and analysis, decision to publish, or preparation of the manuscript.

Author contributions:

Conceptualization: DL, VI, JD, VP, IK. Data curation: DL, VI. Formal analysis: DL, JD. Funding acquisition: LP, AS, AG, VP, IK. Investigation: DL, VI, JR, AF. Methodology: DL, VI, VP, IK. Project administration: LP, AS, AG, VP, IK. Software: DL. Resources: DL, VI, VP, IK. Supervision: JD, VP, IK. Validation: DL. Visualization: DL, VI, JD, VP, IK. Writing – original draft: DL, JD, VP, IK. Writing – review & editing: DL, VI, JD, AG, VP, IK.

Competing interests:

There are no competing interests to declare.

Data and materials availability:

The data that support the findings of this study, and the code related to this study, are available at the public OSF repository, https://osf.io/56hw7, https://doi.org/10.17605/OSF.IO/56HW7.

Supplementary Information

Supplementary text 1. Supplementary Methods, including Supplementary Tables S1 to S5
Supplementary Figures S1 to S5
Supplementary Movies S1 to S9
Supplementary text 2. Instructions for participants

1 Supplementary Methods

1.1 Optimal dyad strategy

Table S1 | Variables used in section 1.1, and their descriptions.

Variable	Description
A, B	Agent names.
$\vec{a}_i, \vec{b}_i$	Agent positions at the start of cycle i.
$\vec{s}_i$	Single target position at the start of cycle i.
$\vec{j}_i^A$	Predominantly blue joint target (higher payoff share for agent A) position at the start of cycle i.
$\vec{j}_i^B$	Predominantly orange joint target (higher payoff share for agent B) position at the start of cycle i.
D_S	Relevant distance for the single target.
D_J	Relevant distance for a joint target.
D	Shortest relevant distance.
w	Target-type weighting parameter, weights single vs joint targets.
$\vec{t}_{i+1}$	Target position updating rule.
$\vec{x}_{i+1}$	Agent position updating rule.
$\vec{y}_{i+1}$	Extended agent position updating rule with advantageous placement.
N	Total number of collection cycles.
Φ	Fraction of single targets collected.

To establish an analytical foundation, we derive the optimal strategy for a dyad that maximizes their joint payoff. We assume for simplicity agents with identical speed, making the Euclidean distances from agents' positions $\vec{a}$ and $\vec{b}$ to the targets $\vec{s}, \vec{j}^A, \vec{j}^B$ the sole determinant of the payoff per second for each target choice. Given that the collection process of a single target begins when the first agent reaches it, the relevant distance for single targets D_S is the minimum distance between the agents and the target:

$$D_S(\vec{a}, \vec{b}, \vec{s}) = \min(||\vec{a} - \vec{s}||, ||\vec{b} - \vec{s}||). \tag{1}$$

Conversely, for joint targets, the collection process starts when the last agent arrives, so the relevant distance D_J is the maximum distance between the agents and the target:

$$D_J(\vec{a}, \vec{b}, \vec{j}^X) = \max(||\vec{a} - \vec{j}^X||, ||\vec{b} - \vec{j}^X||). \tag{2}$$

To maximize the joint payoff, we assume the dyad always selects the target with the shortest relevant distance D:

$$D(\vec{a}, \vec{b}, \vec{s}, \vec{j}^A, \vec{j}^B, w) = \min \begin{cases} D_S(\vec{a}, \vec{b}, \vec{s}) \cdot (1 - w) \\ D_J(\vec{a}, \vec{b}, \vec{j}^A) \cdot w \\ D_J(\vec{a}, \vec{b}, \vec{j}^B) \cdot w \end{cases}, \tag{3}$$

where w is a target-type weighting parameter. When $w = 1/2$, both target types are equally weighted, approximating the optimal dyad strategy. For $w \neq 1/2$, we obtain a non-optimal strategy that approximates the best strategy among those collecting the same fraction of single targets (FST value).

To simulate this strategy, we define the initial agent positions at the center of the game field:

$$\vec{a}_0 = \vec{b}_0 = \begin{pmatrix} 1/2 \\ 1/2, \end{pmatrix} \tag{4}$$

and sample the initial positions of the three targets from the two-dimensional standard uniform distribution:

$$\vec{s}_0, \vec{j}_0^A, \vec{j}_0^B \sim \mathcal{U}^2_{[0,1]}. \tag{5}$$

We define the target position updating rule $\vec{t}_{i+1}$ as implemented in the game

$$\vec{t}_{i+1} = \begin{cases} \vec{u} \sim \mathcal{U}^2_{[0,1]} & \text{if } \vec{t}_i \text{ was collected} \\ \vec{t}_i & \text{otherwise.} \end{cases} \tag{6}$$

If a target is collected, its new position is sampled from the two-dimensional standard uniform distribution $\mathcal{U}^2_{[0,1]}$; otherwise, it remains unchanged. In the first analysis of the optimal strategy, we assume both agents share the same position at the beginning of a collection cycle, defining the agent position updating rule $\vec{x}_{i+1}$ such that they are always at the previously collected target's position at the start of each collection cycle:

$$\vec{x}_{i+1} = \begin{cases} \vec{s}_i & \text{if } \vec{s}_i \text{ was collected} \\ \vec{j}_i^A & \text{if } \vec{j}_i^A \text{ was collected} \\ \vec{j}_i^B & \text{otherwise.} \end{cases} \tag{7}$$

With these updating rules, we can simulate each dyad strategy and thus calculate the expected fraction of single targets Φ:

$$\mathbb{E}[\Phi|w] = \lim_{N\to\infty} \frac{1}{N} \sum_{i=0}^{N} \begin{cases} 1 & \text{if } \vec{s}_i \text{ was collected} \\ 0 & \text{otherwise.} \end{cases} \tag{8}$$

and the expected relevant distance:

$$\mathbb{E}[D|w] = \lim_{N\to\infty} \frac{1}{N} \sum_{i=0}^{N} D(\vec{a}_i, \vec{b}_i, \vec{s}_i, \vec{j}_i^A, \vec{j}_i^B, w), \tag{9}$$

which is proportional to the payoff per second (see the gray curve in Fig. 3b for simulation results).

To relax the initial assumption of agents always sharing the same position at the start of each collection cycle, we extend the agent position updating rule: after collecting a joint target, both agents inevitably share a similar position, therefore, the updating rule remains in this case unchanged. However, during a single target collection, the non-collecting agent can position itself advantageously for the next collection cycle. Thus, we introduce an extended agent position updating rule $\vec{y}_{i+1}$:

$$\vec{y}_{i+1} = \begin{cases} \hat{\vec{y}}_{i+1} & \text{if } \vec{s}_i \text{ was collected by the other agent, and} \\ \vec{x}_{i+1} & \text{otherwise.} \end{cases} \tag{10}$$

This advantageous placement $\hat{\vec{y}}_{i+1}$ minimizes the expected relevant distance:

$$\hat{\vec{y}}_{i+1} = \arg\min_{\vec{y}} \mathbb{E}[D|\vec{x}_{i+1}, \vec{y}, \vec{j}_i^A, \vec{j}_i^B, w]. \tag{11}$$

Note here that $\vec{x}_{i+1} = \vec{s}_i$ since the previous collection was a single target collection. The expected relevant distance equals the integral over all possible single target spawn positions:

$$\mathbb{E}[D|\vec{x}, \vec{y}, \vec{j}^A, \vec{j}^B, w] = \int_{[0,1]^2} D(\vec{x}, \vec{y}, \vec{s}, \vec{j}^A, \vec{j}^B, w) d\vec{s}. \tag{12}$$

Fig. 3b (black curve) illustrates the simulation results with advantageous placement, and Fig. 3d and Fig. S1 depict the expected relevant distances for various free-agent placements.

By simulating strategies for various $w \in [0, 1]$, we establish a function that maps target choices to FST values, $w \mapsto \Phi$ (Fig. S2). Inverting this function allows us to predict dyads' target choices based on their FST value Φ and the current game configuration $\vec{a}_i, \vec{b}_i, \vec{s}_i, \vec{j}_i^A, \vec{j}_i^B$. The subsequent section will delve deeper into modeling dyad strategies.

1.2 Modeling dyad strategies

Table S2 | Variables used in section 1.2, and their descriptions.

Variable	Description
j	Index of collection type. Possible values: 1 ⇔ single target collection, 2 ⇔ predominantly blue joint target collection, and 3 ⇔ predominantly orange joint target collection.
$\hat{y}_j^{(i)}$	Predicted probability for target collection j in collection cycle i.
Softmax	Softmax function.
$\boldsymbol{\theta}$	Regression coefficient matrix.
$\vec{x}^{(i)}$	Covariates of collection cycle i.
$\vec{x}_d$	Covariate component containing the relevant distances for the single and joint targets. The collection cycle i is omitted for simplicity.
$\vec{x}_p$	Covariate component encoding the identity of the previously collected target, whether an invite is present, and towards which joint target the invite is directed. The collection cycle i is omitted for simplicity.
$\vec{x}_{p'}$	Covariate component encoding the identity of the target collected before the previous one. The collection cycle i is omitted for simplicity.
$\boldsymbol{\theta}_d$	Component of the regression coefficient matrix that weights the relevant distance of the single target against those of the joint targets.
d_0	Regression coefficient of the single target's relevant distance.
d_1	Regression coefficient of the joint targets' relevant distances.
$\boldsymbol{\theta}_p$	Component of the regression coefficient matrix encoding either (1) if there is no invite, the relative change in collection probability of the previously collected target, or (2) if an invite is present, the relative change in collection probability of the joint target towards which the invitation is directed.
p_0	Regression coefficient for the change in the collection probability of the single target relative to others if the previous target was a single target.
p_1	Regression coefficient for the change in the collection probability of a joint target relative to others if the previous target was this joint target.
p_2	Regression coefficient for the change in the collection probability of a joint target relative to others if an invite towards this joint target is present.
$\boldsymbol{\theta}_{p'}$	Component of the regression coefficient matrix encoding the relative change in collection probability of the target collected before the previously collected target.
p_3	Regression coefficient for the relative change in the collection probability of the target collected before the previous one. This coefficient accounts for both single and joint targets.
$\mathcal{L}$	Negative log-likelihood function of the generalized linear model (GLM). It is the Cross-Entropy loss.
N	Total number of collection cycles.
$y_j^{(i)}$	Binary encoding indicating whether target collection j occurred in collection cycle i.

For each individual dyad, we fit a generalized linear model (GLM) to obtain predictions $\hat{y}_j^{(i)}$ about the probability for each possible target collection $j \in \{1, 2, 3\}$ given the collection cycles i's covariates $\vec{x}^{(i)}$ and dyads fitted regression coefficients $\boldsymbol{\theta}$

$$\hat{y}_j^{(i)} = \text{Softmax}(\boldsymbol{\theta}^T \cdot \vec{x}^{(i)})_j, \tag{13}$$

where the softmax function is employed to transform the linear combination of covariates $\boldsymbol{\theta}^T \cdot \vec{x}^{(i)}$ into a probability distribution over the target choices $j \in \{1, 2, 3\}$

$$\text{Softmax}(\vec{x})_j = \frac{\exp(x_j)}{\sum_{k=1}^{3} \exp(x_k)}. \tag{14}$$

The covariates $\vec{x}^{(i)}$ for each collection cycle i consist out of three stacked components

$$\vec{x} = \begin{bmatrix} \vec{x}_d \\ \vec{x}_p \\ \vec{x}_{p'} \end{bmatrix}. \tag{15}$$

The first component $\vec{x}_d$ encodes the relevant distances to the targets as in section 1.1

$$\vec{x}_d = \begin{pmatrix} D_S(\vec{a}, \vec{b}, \vec{s}) \\ D_J(\vec{a}, \vec{b}, \vec{j}^A) \\ D_J(\vec{a}, \vec{b}, \vec{j}^B) \end{pmatrix}. \tag{16}$$

The second component $\vec{x}_p$ encodes the end result of the previous cycle as a one-hot-encoded vector. This encompasses: (1) which target was collected and if it was a single target, (2) whether there is an invite (as defined in section 1.3), and if there is an invite, then towards which of the two joint targets it is.

$$\vec{x}_p = \begin{cases} \begin{pmatrix} 1 & 0 & 0 & 0 & 0 \end{pmatrix}^T & \text{if } \vec{s} \text{ previously collected and no invite,} \\ \begin{pmatrix} 0 & 1 & 0 & 0 & 0 \end{pmatrix}^T & \text{if } \vec{j}^A \text{ previously collected,} \\ \begin{pmatrix} 0 & 0 & 1 & 0 & 0 \end{pmatrix}^T & \text{if } \vec{j}^B \text{ previously collected,} \\ \begin{pmatrix} 0 & 0 & 0 & 1 & 0 \end{pmatrix}^T & \text{if } \vec{s} \text{ previously collected and invite towards } \vec{j}^A, \\ \begin{pmatrix} 0 & 0 & 0 & 0 & 1 \end{pmatrix}^T & \text{if } \vec{s} \text{ previously collected and invite towards } \vec{j}^B. \end{cases} \tag{17}$$

The third and last component encodes, also as a one-hot-encoded vector, which target type was collected two cycles ago.

$$\vec{x}_{p'} = \begin{cases} \begin{pmatrix} 1 & 0 & 0 \end{pmatrix}^T & \text{if } \vec{s} \text{ collected prior to the previously collected, i.e., two cycles ago,} \\ \begin{pmatrix} 0 & 1 & 0 \end{pmatrix}^T & \text{if } \vec{j}^A \text{ collected prior to the previously collected,} \\ \begin{pmatrix} 0 & 0 & 1 \end{pmatrix}^T & \text{if } \vec{j}^B \text{ collected prior to the previously collected.} \end{cases} \tag{18}$$

Analogous to the covariates $\vec{x}$ the coefficient matrix $\boldsymbol{\theta}$ consists out of three stacked components

$$\boldsymbol{\theta} = \begin{bmatrix} \boldsymbol{\theta}_d \\ \boldsymbol{\theta}_p \\ \boldsymbol{\theta}_{p'} \end{bmatrix}. \tag{19}$$

Where the first component $\boldsymbol{\theta}_d$ weights the relevant distance of the single target against those of the joint targets similar as the weighting w in section 1.1

$$\boldsymbol{\theta}_d = \begin{pmatrix} d_0 & 0 & 0 \\ 0 & d_1 & 0 \\ 0 & 0 & d_1 \end{pmatrix}. \tag{20}$$

The second component $\boldsymbol{\theta}_p$ does change either the relative probability of the previously collected target to the others or, if an invite is present, changes the relative probability of the joint target towards the invite is

$$\boldsymbol{\theta}_p = \begin{pmatrix} p_0 & 0 & 0 \\ 0 & p_1 & 0 \\ 0 & 0 & p_1 \\ 0 & p_2 & 0 \\ 0 & 0 & p_2 \end{pmatrix}. \tag{21}$$

The last component $\boldsymbol{\theta}_{p'}$ allows for a dependence further into the past. It modulates the probability of the next target towards the identity of the target prior to the previous target:

$$\boldsymbol{\theta}_{p'} = \begin{pmatrix} p_3 & 0 & 0 \\ 0 & p_3 & 0 \\ 0 & 0 & p_3 \end{pmatrix}. \tag{22}$$

Note that here in this component, the model does not differentiate between single and joint targets. To obtain the coefficient matrix $\boldsymbol{\theta}$, we use the quasi-Newton BFGS algorithm to minimize the negative log-likelihood function

$$\mathcal{L} = -\sum_{i=1}^{N}\sum_{j=1}^{3} y_j^{(i)} \ln(\hat{y}_j^{(i)}), \tag{23}$$

where $y_j^{(i)}$ is a binary encoding whether target collection j happened in collection cycle i or not and $\hat{y}_j^{(i)}$ is, as defined previously, the corresponding predicted probability of this target collection. The resulting prediction accuracy for unseen data (visualized in Fig. 4a) is evaluated for all collection cycles of the stable period (minutes 10–40) with k-fold cross-validation ($k = 5$).

With this model, we can not only predict the dyad's target choice but we do also obtain an estimate of the dyad's uncertainty about the target choice at the start of the collection cycle (as utilized in Fig.5b and c). We estimate the dyads uncertainty with the uncertainty of our model which is quantified by the Shannon entropy H of the model's target prediction:

$$H(i) = -\sum_{j=1}^{3} \hat{y}_j^{(i)} \log_2(\hat{y}_j^{(i)}). \tag{24}$$

1.3 Trajectory classification

Trajectory classification is performed by a procedural algorithm that assigns a trajectory class (see Fig. 5a for visualizations) to each collection cycle based on a set of predefined conditions. The thresholds used in these conditions are set manually, and the trajectory classes are evaluated in a predetermined order. If a condition is met, the corresponding trajectory class is assigned to the cycle, and the algorithm proceeds to the next condition only if the current one is not met.

The first trajectory class evaluated is the "Invitation" class. A collection cycle is classified as "Invitation" if it follows a single target collection in the previous cycle, during which the non-collecting agent positioned itself in an "inviting" manner, that is, near a joint target before the collection of the previous single target collection is completed. This inviting placement can be either on the joint target (on-target-invite) or nearby the joint target (nearby-target-invite), with the latter defined as a distance less than half of that from the other agent. If the joint target is collected subsequently, the cycle is classified as "Invitation" otherwise, it is classified as "Failed invitation". If the nearby-target-invite condition is met, a cycle is only classified as "Failed invitation" if the overall FST is below 2/3, otherwise, it is more probable that the placement near the joint target is a coincidence. If neither the on-target-invite nor the nearby-target-invite condition is met, the algorithm proceeds to evaluate the "Strongly curved" trajectory class.

A collection cycle is classified as "Strongly curved" if the fraction of the excess trajectory length due to curvature exceeds 0.32. If this condition is not met, the agents' trajectories are relatively straight and the algorithm proceeds evaluating the condition of the "Different targets" trajectory class.

To determine whether the two agents aimed for different targets or the same, the algorithm fits straight lines to their trajectories, which serves to (1) smooth out the motor noise and (2) extend the aim of the agent beyond the final position reached. For each agent, the algorithm checks (1) whether the agent moved towards a target and (2) whether this target is in proximity

to the corresponding line (i.e., less than 10.14 cm). If a target meets these conditions, it is considered a potential candidate for the agent's aim. If multiple candidate targets exist, the algorithm selects the one closest to the agent's final position after weighting the distances from the agents to the candidates according to the overall FST. This results in a prediction of which target each agent aimed for. If these predictions differ, the cycle is classified as "Different targets". Note that if both agents initially aimed at different joint targets, the collection cycle would not end, leading to curved trajectories, which is why different initial aims towards joint targets are subsumed under the "Strongly curved" trajectory class.

Finally, the algorithm checks whether one agent moves ahead towards the target at which both agents aim. If the difference in distance averaged over the collection cycle to the finally collected target exceeds 3.4 cm, the cycle is classified as "One ahead". If none of the above conditions hold true, the cycle is classified as "Concurrent" by exclusion principle.

1.4 Joint payoff

Table S3 | Variables used in section 1.4, and their descriptions.

Variable	Description
R	Joint payoff.
N	Number of target collections / collection cycles.
r	Payoff per target (7 cents).
T	Block duration (20 minutes).
t_i^{acq}	Duration of the acquisition period in cycle i.
$\langle\rangle$	Mean over all cycles.
t^{col}	Duration of the collection period (1 second).
e_1, e_2	Approximation errors.
l_i	Limiting trajectory length in cycle i.
s_i	Mean agent speed on the limiting trajectory in cycle i.
l_i^C	Additional trajectory length due to curvature in cycle i.
d_i	Limiting distance in cycle i.
d_i^T	Distance between the previous and the next target in cycle i.
d_i^R	Distance reduction due to advantageous placement in cycle i.

To elucidate the of role spatiotemporal factors in addition of those of classical discrete decision-making, we analyze in more detail the factors that determine the joint payoff of a dyad, using as a basis the observed trajectories of the dyads (Fig. 6). The joint payoff R equals the total number of target collections N times the payoff per target $r = 7$ cent

$$R = rN. \tag{25}$$

The total number of target collections N can be approximated by dividing the duration of each block $T = 20$ minutes by the mean collection cycle duration. The latter is the sum of the mean acquisition period duration $\langle t^{\mathrm{acq}}\rangle$ and the constant collection period duration $t^{\mathrm{col}} = 1$ second:

$$R = rN = r\frac{T}{\langle t^{\mathrm{acq}}\rangle + t^{\mathrm{col}}} + e_1. \tag{26}$$

The approximation error is denoted as e_1 and negligible ($r = 0.99, p < 10^{-6}$). The duration of an acquisition period t_i^{acq} equals the length of the so-called *limiting trajectory length* l_i divided by the corresponding speed on this trajectory s_i:

$$t_i^{\mathrm{acq}} = \frac{l_i}{s_i}. \tag{27}$$

The length of the limiting trajectory l_i is either equal to the trajectory length of agent A or agent B. In case of a single target collection, it is that of the collecting agent, and in case of a joint target collection, it is that of the agent that entered last:

$$l_i = \begin{cases} l_i^A & \text{if } \vec{s}_i \text{ collected by agent } A, \\ l_i^B & \text{if } \vec{s}_i \text{ collected by agent } B, \\ l_i^A & \text{if } \vec{j}_i^X \text{ collected and agent } A \text{ entered last,} \\ l_i^B & \text{if } \vec{j}_i^X \text{ collected and agent } B \text{ entered last.} \end{cases} \tag{28}$$

By approximating the mean acquisition period duration $\langle t^{\text{acq}} \rangle$, we show that the joint payoff R is approximately proportional to the mean speed on and mean length of the limiting trajectory:

$$R = rN = r\frac{T}{\langle t^{\text{acq}} \rangle + t^{\text{col}}} + e_1 = r\frac{T}{\frac{\langle l \rangle}{\langle s \rangle} + t^{\text{col}}} + e_2. \tag{29}$$

The increased error, quantified by $e_2 > e_1$, originates from the inequality of the mean of a ratio to the ratio of means $\langle x/y \rangle \neq \langle x \rangle / \langle y \rangle$. Despite the increase, the error in predicting the joint payoff R remains negligible ($r = 0.99, p < 10^{-6}$). To decompose the joint payoff R further, we denote that the length of the limiting trajectory l is the sum of the excess length due to curvature l_i^C and the so-called *limiting distance* d_i.

$$l_i = l_i^C + d_i \tag{30}$$

The limiting distance d_i is the straight-line distance from the initial position of the limiting trajectory to the collected target. The limiting distance d_i results out of the position of the previously collected target and the amount of advantageous agent placement. Therefore, the limiting distance d_i is equal to the distance from the position of the previously collected target to the position of the subsequently collected target d_i^T minus the distance reduction due to advantageous placement d_i^R (see section 1.1)

$$l_i = l_i^C + d_i = l_i^C + d_i^T - d_i^R. \tag{31}$$

Substituting this into our joint payoff estimate, we observe its dependence on four variables:

$$R = rN = r\frac{T}{\langle t^{\text{acq}} \rangle + t^{\text{col}}} + e_1 = r\frac{T}{\frac{\langle l \rangle}{\langle s \rangle} + t^{\text{col}}} + e_2 = r\frac{T}{\frac{\langle l^C \rangle + \langle d^T \rangle - \langle d^R \rangle}{\langle s \rangle} + t^{\text{col}}} + e_2. \tag{32}$$

Here the error e_2 remains unchanged as the means of equal sample sizes are added. Two of the four variables (d^T and d^R) could in principle result out of classical discrete decision-making. The other two (l^C and s), however, result out of continuous, spatiotemporal interactions. Altogether, they shape the joint payoff in the cooperation–competition foraging game.

1.5 Individual payoffs

After analysing the joint payoff's dependencies, we proceed to decompose the individual payoff of a generic agent X and its counterpart, agent Y. We begin with two key relationships. We utilize (1) that the half of the joint payoff $R/2$ is exactly the within-dyad mean agent's individual payoffs (R^X and R^Y)

$$\frac{R^X + R^Y}{2} = \frac{R}{2} \tag{33}$$

and (2) that the difference from this intermediate payoff $R/2$ to the individual payoff R^X of an agent X equals the half of the inter-agent payoff difference $R_\Delta^X/2$ (defined later)

$$R^X = \frac{R}{2} + \frac{R_\Delta^X}{2}. \tag{34}$$

Table S4 | Variables used in section 1.5, and their descriptions.

Variable	Description
X, Y	Generic agent names, could be either the blue or the orange target. If a variable is defined for agent X, the definition for agent Y is analogous.
R^X	Individual payoff of agent X.
R^X_Δ	Payoff difference of agent X to the other agent Y. Note that $R^X_\Delta = -R^Y_\Delta$.
n^X_s	Number of single target collections by agent X.
n^X_j	Number of joint target collections with a higher payoff share for agent X.
r_s	Payoff for a single target collection (7 cents).
$\hat{r}_j$	Higher payoff share of a joint target collection (5 cents).
$\check{r}_j$	Lower payoff share of a joint target collection (2 cents).
e	Error of predicting the payoff difference using only the single target difference. It is equal to the payoff difference due to differences in joint target type collections.

We observe that the individual payoff R^X depends on the payoff difference R^X_Δ and on the joint payoff R. From the previous section, we know on what variables the joint payoff R depends. Subsequently, we here analyze which variable is responsible for the inter-agent payoff difference

$$R^X_\Delta = R^X - R^Y. \tag{35}$$

The individual payoffs can be decomposed by the type of target:

$$R^X = n^X_s r_s + n^X_j \hat{r}_j + n^Y_j \check{r}_j \tag{36}$$

and

$$R^Y = n^Y_s r_s + n^Y_j \hat{r}_j + n^X_j \check{r}_j, \tag{37}$$

where n^X_s is the number of single target collections of agent X and $r_s = 7$ cent the payoff for a single target collection. n^X_j is the number of collected joint targets with a higher payoff share for agent X. This higher payoff share is $\hat{r}_j = 5$ cent. The lower joint target payoff share $\check{r}_j$ is 2 cents. The variables for agent Y are defined analogously. By substituting these calculations into our payoff difference formula we obtain:

$$R^X_\Delta = R^X - R^Y = (n^X_s - n^Y_s)r_s + (n^X_j - n^Y_j)(\hat{r}_j - \check{r}_j). \tag{38}$$

The right hand side of this equation has two components. The first, $(n^X_s - n^Y_s)r_s$, accounts for the payoff difference due to differences in single target collections. The second component, $(n^X_j - n^Y_j)(\hat{r}_j - \check{r}_j)$, accounts for the payoff difference due to difference in joint target collections. By leaving out the latter and introducing an error term e, we approximate the payoff difference

$$R^X_\Delta = R^X - R^Y = (n^X_s - n^Y_s)r_s + e \tag{39}$$

only with the difference in single targets. By demonstrating that the error e is negligible, we confirm that the inter-agent payoff difference is shaped predominantly by the difference in single targets (as visualized in Fig. 7b, $r = 0.99, p < 10^{-6}$). Thus, the individual payoff R^X depends on the four variables known from previous section and on a fifth variable, the difference in single target collections between the agents.

1.6 Estimating the optimal strategy and cost of cooperation

We show that participants are more cooperative than optimal and pay an associated cost of cooperation — the loss of income because of the choice of a non-optimal, overly cooperative, strategy. To estimate this cost of cooperation we estimate for each individual agent X the optimal strategy taking into account their estimated relative skill level. This optimal strategy is the strategy that maximizes the agent X's expected individual payoff. To predict this expected

Table S5 | Variables used in section 1.6, and their descriptions.

Variable	Description
Φ	Fraction of single targets (FST).
$\tilde{S}^X_\Delta$	Sensorimotor skill difference. It is the normalized single target difference S^X_Δ, considering only single target collections that are not due to defections like the "Different targets" and "Failed invitation" trajectory classes.
S^X_Δ	Normalized single target difference. It represents the difference in single target collections between agent X and agent Y, divided by the total number of single target collections. Note that $S^X_\Delta = -S^Y_\Delta$.
$\hat{R}^X(\Phi, \tilde{S}^X_\Delta)$	Estimated individual payoff of agent X given Φ and $\tilde{S}^X_\Delta$.
$\hat{R}(\Phi)$	Estimated joint payoff given Φ.
$\hat{R}^X_\Delta(\Phi, \tilde{S}^X_\Delta)$	Estimated inter-agent payoff difference for agent X given Φ and $\tilde{S}^X_\Delta$. Note that $\hat{R}^X_\Delta(\Phi, \tilde{S}^X_\Delta) = -\hat{R}^Y_\Delta(\Phi, \tilde{S}^Y_\Delta)$.
$\hat{\Phi}^X(\tilde{S}^X_\Delta)$	Estimated fraction of single targets of the optimal strategy of agent X given their skill difference $\tilde{S}^X_\Delta$.
$C(\Phi, \tilde{S}^X_\Delta)$	Estimated cost of cooperation for the higher-skilled agent X. It is called the cost of cooperation since the optimal strategy for a sufficiently higher-skilled agent is pure competition ($\Phi = 1$).

individual payoff, we model the individual payoff R^X of agent X as a function of FST Φ and skill difference $\tilde{S}^X_\Delta$ (defined later) analogous to the formula in section 1.5:

$$\hat{R}^X(\Phi, \tilde{S}^X_\Delta) = \frac{\hat{R}(\Phi)}{2} + \frac{\hat{R}^X_\Delta(\Phi, \tilde{S}^X_\Delta)}{2}, \tag{40}$$

where we use (1) an estimate of the inter-agent payoff difference $\hat{R}^X_\Delta(\Phi, \tilde{S}^X_\Delta)$ and (2) an estimate of the joint payoff $\hat{R}(\Phi)$. The latter follows out of an estimate of the number of target collections $\hat{N}(\Phi)$ which is analogous to that in section 1.4

$$\hat{R}(\Phi) = r\hat{N}(\Phi) = r\frac{T}{\frac{\hat{l}^C(\Phi)+\hat{d}^T(\Phi)-\hat{d}^R(\Phi)}{\hat{s}(\Phi)} + t^{\text{col}}}. \tag{41}$$

The four dependencies, $\hat{l}^C(\Phi), \hat{d}^T(\Phi), \hat{d}^R(\Phi)$ and $\hat{s}(\Phi)$, of the joint payoff R are here estimated by fitting low-degree polynomials. This is a modeling choice to obtain later on the expected cost of cooperation for the average dyad. Alternatively, one could use here the values and assumptions from section 1.1 to obtain the cost of not pursuing the optimal dyad strategy. Having now defined the estimate for the joint payoff $\hat{R}(\Phi)$ we now continue with the estimate of the inter-agent payoff difference $\hat{R}^X_\Delta(\Phi, S^X_\Delta)$. Therefore, reusing the estimate from section 1.5:

$$R^X_\Delta = r_s(n^X_s - n^Y_s) + e \tag{42}$$

by multiplying $1 = \frac{N\Phi}{n^X_s + n^Y_s}$ we obtain

$$R^X_\Delta = r_s N\Phi \frac{n^X_s - n^Y_s}{n^X_s + n^Y_s} + e, \tag{43}$$

which motivates the definition of the normalized single target difference

$$S^X_\Delta = \frac{n^X_s - n^Y_s}{n^X_s + n^Y_s}. \tag{44}$$

This measure quantifies the efficiency of agent X in contrast to that of agent Y to collect single targets independently of FST. To make this measure generalizable to differing FST values, we exclude those single target collections due to defections ("Different targets" and "Failed

invitation" trajectory classes from section 1.3) to obtain the sensorimotor *skill difference* $\tilde{S}^X_\Delta$. Now we define our new estimate of the inter-agent payoff difference as

$$\hat{R}^X_\Delta(\Phi, \tilde{S}^X_\Delta) = r\hat{N}(\Phi)\Phi\tilde{S}^X_\Delta, \tag{45}$$

where we utilize again our estimate of the number of target collections $\hat{N}(\Phi)$. Combining our estimate of the inter-agent payoff difference $\hat{R}^X_\Delta(\Phi, \tilde{S}^X_\Delta)$ with that of the joint payoff $\hat{R}(\Phi)$ we estimate agent X's individual payoff $\hat{R}^X(\Phi, \tilde{S}^X_\Delta)$ with high accuracy ($r = 0.88, p < 10^{-6}$) given only the FST Φ and the skill difference $\tilde{S}^X_\Delta$ (see Fig. 7c). Now we can estimate the FST value of agent X's optimal strategy

$$\hat{\Phi}^X(\tilde{S}^X_\Delta) = \arg\max_\Phi \hat{R}^X(\Phi, \tilde{S}^X_\Delta) \tag{46}$$

as well as the cost of cooperation of the higher-skilled agent X

$$C(\Phi, \tilde{S}^X_\Delta) = \max_\Phi(\hat{R}^X(\Phi, \tilde{S}^X_\Delta)) - \hat{R}^X(\Phi, \tilde{S}^X_\Delta) \tag{47}$$

for a given skill difference $\tilde{S}^X_\Delta$ (Fig. 7d).

Supplementary Figures

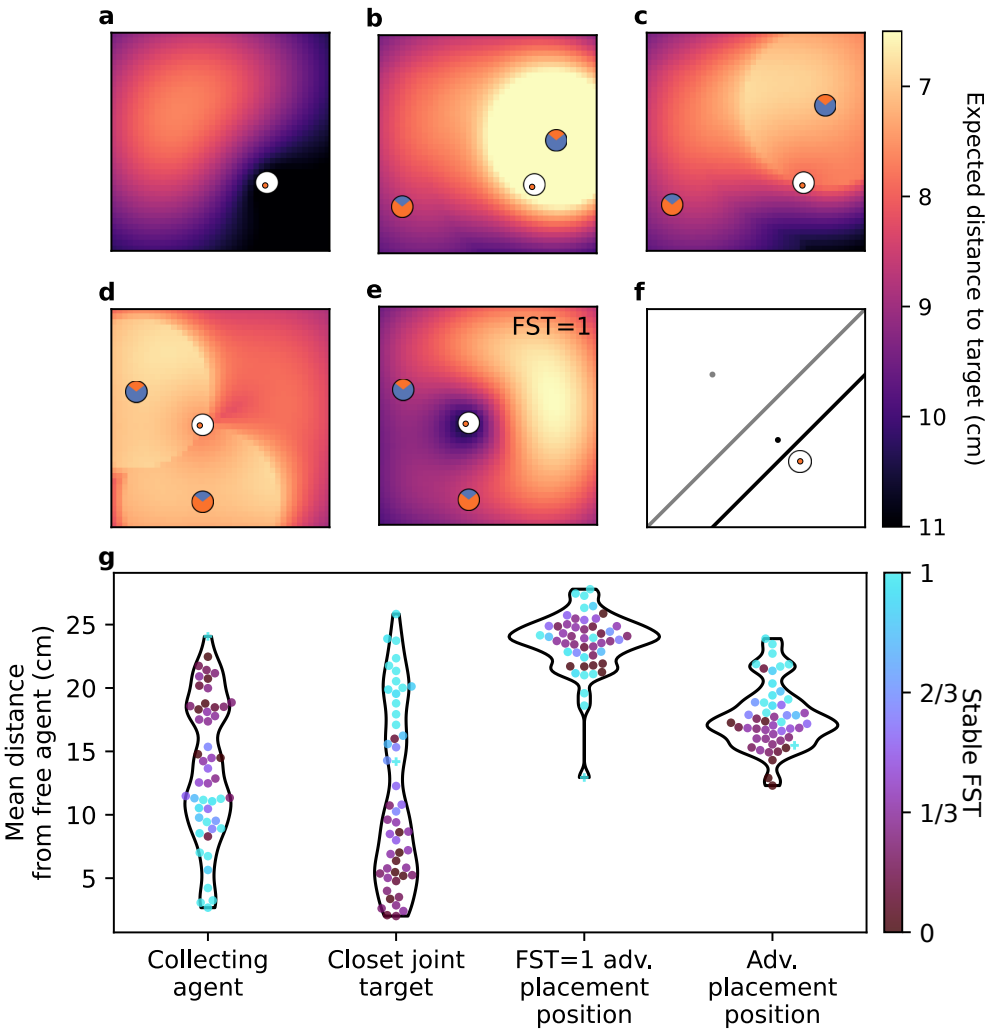

Fig. S1 | Advantageous placement, competitive placement and actual placement during single target collections. (**a-e**) Examples illustrating optimal (advantageous) placement of the non-collecting agent to minimize the average expected distance to the next collected target of *both* agents (colormap). (**a**) Assuming no joint targets, the advantageous placement is on the other half of the game field. (**b**) When including joint targets, the advantageous placement lies approximately within a circle centered on the closest joint target and extending to include the currently collecting agent. (**c**) When the closest joint target is further away, it becomes apparent that the corresponding circle includes the optimum splitting the game field between the two agents, as in (a). (**d**) In some target configurations, large parts of the game field are near optimal. (**e**) For a FST=1 dyad, the optimal placement does not depend on the joint targets. (**f**) Competitive placement example. The black dot represents a competitive placement, where the free, non-collecting agent optimizes the partitioning of the game field such that their probability of getting the next single target is maximized. For comparison, the gray dot represents the non-competitive advantageous placement as in (a) and the gray line indicates the corresponding split of the game field into two parts. (**g**) Actual mean distance of the free, non-collecting agent to four positions: (i) that of the collecting agent, (ii) that of the closest joint target, and (iii-iv) to the advantageous placement in a FST=1 and in optimal contexts. Instead of performing advantageous placement, agents in FST ≥ 0.9 dyads perform, by placing themselves close to the collecting agent, competitive placement and agents in $0.1 <$ FST < 0.9 dyads place themselves close to the closest joint target. Note that FST ≤ 0.1 dyads are excluded since single target collections are sparse.

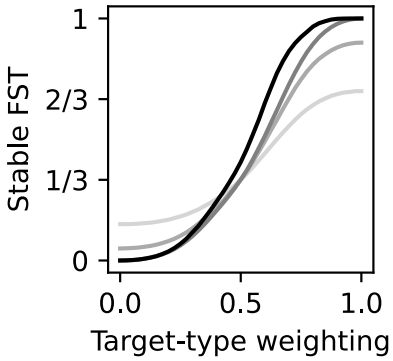

Fig. S2 | **Cooperation–competition weighting of distances.** To achieve different FSTs (fraction of single targets), the simulation requires different weightings of distances w reflecting specific dyads' preferences for selecting single targets vs. joint targets (eq. (3)). The black curve assumes an optimal "advantageous" placement of the non-collecting agent when the partner collects the single target, the dark gray curve assumes that the agents always move together and always select nearest (weighted) target, and the lighter gray lines assume non-optimal agents who move together but select a target randomly in 10% or 30% of trials (corresponding to the light gray lines in Fig. 3d).

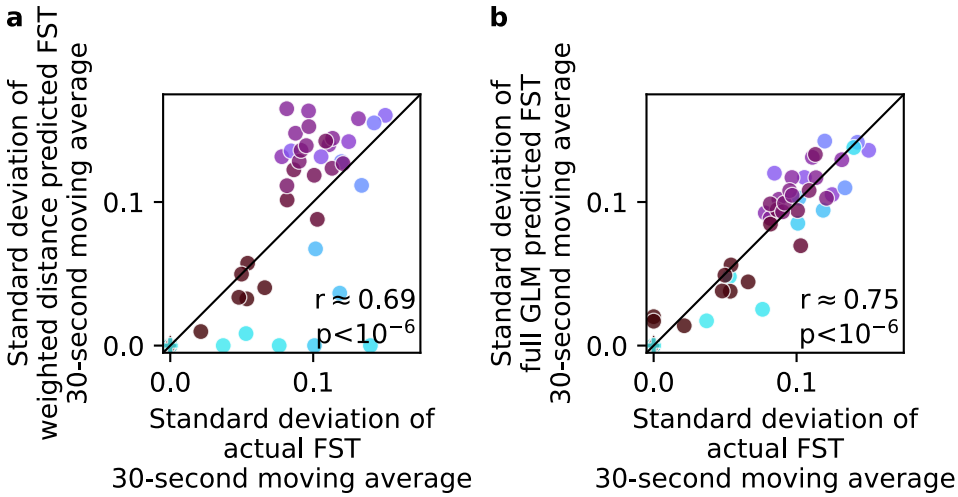

Fig. S3 | **Variance of model predictions.** (**a**) For high FST (light blue dots), the variance of predictions of the weighted distance model is too low whereas it is too high for intermediate FST (purple dots). (**b**) The full GLM is not only more accurate in its predictions (Fig. 4a), but also the variance of the predicted target type timecourse is better correlated with actual variance (Wilcoxon signed-rank test comparing the differences of standard deviations between 30-second moving average FST of the actual and each of the two model's predictions for the 40/58 dyads that exhibit FST fluctuations, $W = 258, p < 0.05, n = 40,$ Mdn$_1 = -0.01\ [-0.03, 0.02],$ Mdn$_2 = 0.0008\ [-0.009, 0.02], r_{rb} = 0.32, CI = [0.04, 0.62]$).

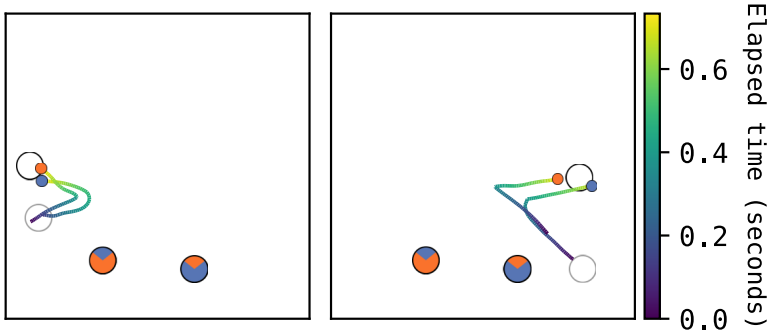

Fig. S4 | **"Go-before-you-know" effect**. Two example trajectories of a FST=1 dyad. Despite the certainty of target choice, the trajectories are strongly curved. Immediately after previous target collection, the agents move in the direction that minimizes the expected distance to the next target (the center of the game field), reflecting a preemptive strategy. Subsequently, once the newly appeared target is perceived, the trajectory is adjusted.

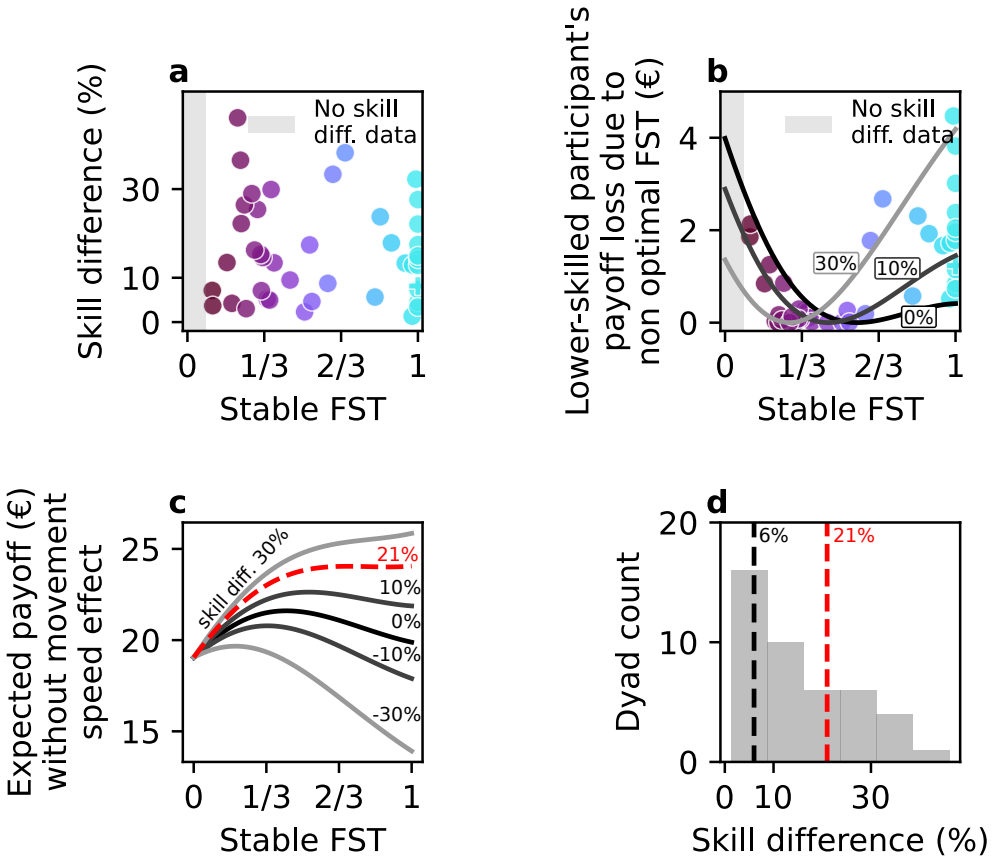

Fig. S5 | **Skill differences and movement speed effect.** (**a**) There is no observed relationship between skill difference in the dyad and the strategy they converged to. (**b**) Often the chosen strategy is also not optimal for the lower-skilled participant (*cf.* Fig. 7d). Note that each participant can increase FST on its own but decrease it only with the compliance of the other. (**c**) Expected payoff without the movement speed effect visualized as in Fig. 7c. The critical value of skill difference at which competition is optimal for the higher-skilled participant without taking into account the movement speed effects is at 21% (red dashed line). (**d**) Comparing the critical skill difference values expected with the movement speed effect (black dashed line) and without the speed effect (red dashed line). Due to the movement speed effect, competition is the best strategy for the majority of higher skilled participants.

Supplementary Movies

[YouTube playlist] — [Open Science Framework movies]

1. **Movie S1:** YouTube or OSF
   Setup and game demonstration. Human Dyadic Interaction Platform setup and the game demonstration (60 s), followed by the replay of an example intermediate dyad.

2. **Movie S2:** YouTube or OSF
   Cooperative example. Replay of a representative dyad from the cooperative group.

3. **Movie S3:** YouTube or OSF
   Intermediate strategy example. Replay of a representative dyad from the intermediate group.

4. **Movie S4:** YouTube or OSF
   Competition example. Replay of a representative dyad from the competitive group.

5. **Movie S5:** YouTube or OSF
   Invitations examples. Collection cycles where one agent invites the other to a joint target.

6. **Movie S6:** YouTube or OSF
   Cooperative turn-taking. Replay of one of three dyads who alternated between the two joint targets.

7. **Movie S7:** YouTube or OSF
   Strongly curved trajectories. Examples of collection cycles featuring strongly curved trajectories, reflecting initial miscoordination and changes of mind.

8. **Movie S8:** YouTube or OSF
   Competitive placement example. Replay of a dyad performing competitive advantageous placement.

9. **Movie S9:** YouTube or OSF
   Cooperative placement for single targets. A special dyad that achieved nearly optimal advantageous placement by splitting the game field.

Instructions for participants

Welcome, and thank you for agreeing to participate in our experiment!
In this experiment you will play a game with another person through a transparent display.

Explanation of the game

In this game you need to collect targets to earn money. At the beginning the experimenter will assign a color to each player (blue and orange). On the screen you will see your own and other player's cursor (small circle colored respectively); you will be able to control your cursor with a computer mouse. The speed of the cursor is limited and by moving the mouse too fast you will have less control over it. To collect a target you need to place the cursor over the target and wait till the target completely disappears. At each time point of the game there will be 3 different targets available on the screen:

1. One white
2. One blue with a share of orange
3. One orange with a share of blue

You can collect white targets on your own - if you are first to select such a target, it becomes unavailable for the other player. To collect the colorful targets you need the other player to select the same target. Each collected target gives you a specific amount of money:

- White target gives 7 cents to the player who got it first
- Blue-orange target gives 5 cents to the blue player and 2 cents to the orange player
- Orange-blue target gives 5 cents to the orange player and 2 cents to the blue player

The amount of money you have collected will be displayed on the right side of the game field.
Structure of the experiment

The experiment will take ca. 2.5 hours in total. First, you will have a short game-tutorial to try out cursor control and target collection. Then, you will play 2 blocks, each 20 minutes, and between the blocks you will have an opportunity to take a break. From the start till the end of the experiment (including the breaks) we ask you to not communicate with the other player. In the end we will ask you to fill out a questionnaire.
Payment

You will receive the money you have collected in one of the blocks. In the end of the experiment, you will roll a dice to randomly select a block accordingly to which you will be paid:

- 1, 2, 3 - first block
- 3, 4, 5 - second block